Cell Micro-Rheology Under Hypergravity Conditions

Sharon van Rijthoven - 4459784
Biomedical Engineering
Delft University of Technology

Supervisors: **Prof.dr. Gijsje Koenderink[1], Dr. ing. Jack J.W.A. van Loon[2,3], and Prof. dr. Thomas Schmidt[4]**

[1]Department of Bionanoscience, Delft University of Technology
[2]Department of Oral and Maxillofacial Surgery/Pathology, Amsterdam Movement Sciences & Amsterdam Bone Center (ABC), Amsterdam UMC location Vrije Universiteit Amsterdam & Academic Center for Dentistry Amsterdam (ACTA)
[3]European Space Agency (ESA), European Space Research and Technology Centre (ESTEC), TEC-MMG
[4]Leiden Instituut Onderzoek Natuurkunde LION - Biological & Soft Matter, Leiden University

April - December 2023

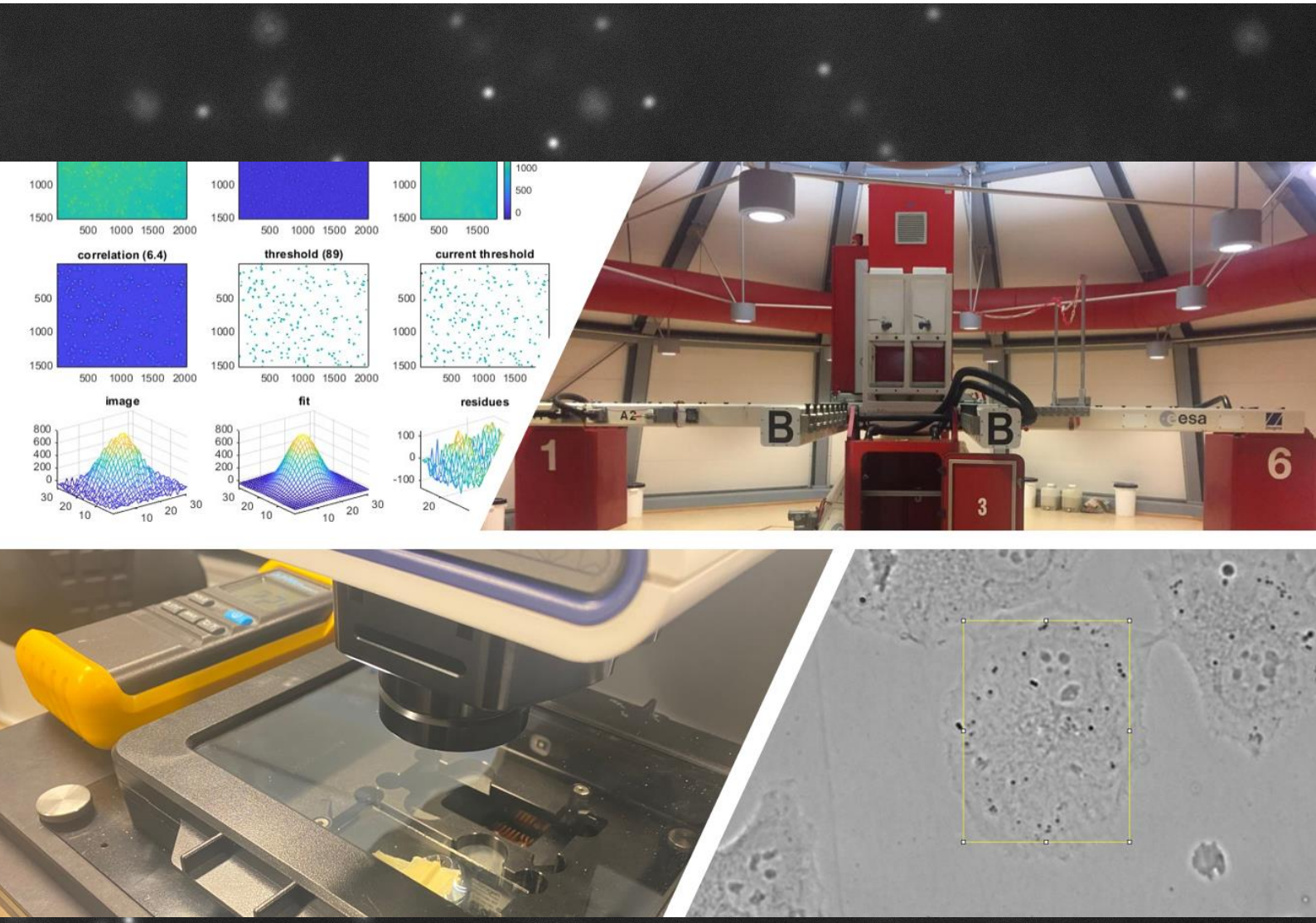

CONTENTS

1 INTRODUCTION

In recent years, it has become progressively evident that not only the biochemical but also the biomechanical environment has a significant role in cell physiology, function, and differentiation[2]. One of the mechanical properties of the cell is the intracellular viscosity which describes the complex, heterogeneous fluidity of the interior of the cell. Alterations in viscosity can greatly change the diffusion rate of biochemicals[3]. As most, if not all, biochemical reactions are to a certain extent diffusion-dependent, their reaction rate can be directly influenced by changes in viscosity[4]. Changes in cellular viscosity have been found in a range of human diseases like diabetes[5] and neurodegenerative diseases like Parkinson's disease[6]. Furthermore, intracellular viscosity changes are also linked to cancer cell migration[7]. In fact, intracellular viscosity is such a significant mechanical property that some species of budding yeast even developed methods to actively control their viscosity[8].

Cell behaviour changes in altered gravity and is suspected to be the source of the macroscale symptoms seen in astronauts[9]. However, it is interesting how a relatively small force at cellular level can have such a detrimental effect, while cells are known to be able to withstand much greater forces generated by the body. We hypothesized that gravity might alter the viscosity in the cell. However, little research to the best of my knowledge have been performed on viscosity in altered gravity. Woodcock et al.[10] mentions increased viscosity in cellular membranes in hypergravity which was also observed by Sieber et al.[11] in SH-SY5Y cells, and Janmaleki et al.[12] indicated decreased viscosity of endothelial cells in simulated microgravity. However, numerous articles do report altered cell stiffness in altered gravity which is related to the viscosity as both describe resistance. While viscosity is a fluid's or gas's resistance to flow, stiffness is a solid's resistance to deform[13]. Viscosity of the cell adds to the perceived cell stiffness. A very viscous fluid inside the cell makes it more difficult to deform that cell compared to a cell with a low viscosity. In simulated microgravity stiffness seems to decrease[12,14-17], while in hypergravity it appears to increase[18].

An ESA research project to the International Space Station, called the MechanoCell, led by Dr. ir. Jack van Loon is planned for launch on a To Be Determined (TBD) launch date, and will investigate cell mechanical properties of MC-3T3 using Single Particle Tracking (SPT) in microgravity. Before the mission can proceed, it must be tested in hypergravity to determine if the selected methods are feasible and if any changes are observed at all in altered gravity. One can imagine that if no differences are observed when changing from 1 to 15 g, no results are expected from 1 g to microgravity either. Hence the objective of this study is to answer the following question:

Does hypergravity alter the viscosity of cells and can this be measured with single particle tracking?

Multiple rheology techniques exist ranging from active techniques like Magnetic Tweezers and Atomic Force Microscopy to passive techniques like Diffusing Wave Spectroscopy, Laser Particle Tracking Microrheology and Single or Multiple Particle tracking. Each technique has its own limitation. While active techniques allow for a larger range of investigated forces, they also apply local stress[19]. Passive techniques do not introduce this stress but injecting probes in the cell is invasive. Using cell structures instead as tracking particles does not induce additional forces or damage to the cell membrane but it is prone to large errors as the particle size, shape and weight cannot be controlled and vary a lot between particles. Single Particle Tracking of cell structures is planned for the MechanoCell mission as it does not require a lot of astronaut interventions.

In this study SPT software, a homemade software developed by Schmidt Lab[20], is applied to endogenous particles in Hela cells experiencing hypergravity in the Large Diameter Centrifuge (LDC) at ESA ESTEC. The software tracks the endogenous particles in the Hela cells by comparing the frames of the video made by the EVOS microscope in the LDC while in hypergravity. The trajectories of the

particles allow to calculate the Mean Square Displacement (MSD). From the MSD the diffusion coefficient can be determined for which the applied function depends on the selected type of diffusion[1]. In this study pure diffusion is assumed such that the Stokes-Einstein equation can be applied to calculate the viscosity. This equation describes how the particle's position changes in response to the solvent molecules colliding with the particle due to random forces created by thermal energy[19]. Prior to performing the experiments with Hela cells, the parameters of the SPT software were optimized and additional thresholds were included to improve the SPT software for endogenous particles, after which the setup was validated with a known sucrose solution.

It is important to acknowledge that the exact values of viscosity derived from this study may not be appropriate for direct implementation. Aside from the large variability in literature which depend on method[21], cell type[22], and even location in the cell[23], many simplifications are made. It is assumed that the cytoplasm behaves as a pure Newtonian fluid in which the particles are free floating and only subjected to normal diffusion. However, in reality, the cell is a complex, heterogenous and crowded environment with interconnected cell structures and processes[24].

The study shows that the SPT software is successful in measuring changes in viscosity in hypergravity. Although the viscosity appears to change in Hela cells, improvements and more research has to be performed to determine if this is a result of hypergravity or due to other factors. For future research it is recommended to include more cells and cell types, cover the time-dependent nature of the mechanical properties of the cell in the viscosity calculations, determine the cell's hypergravity recovery time, actively control temperature and CO_2, minimize the LDC vibrations, and investigate the contribution of the cytoskeleton to the cell viscosity by incorporating cytoskeletal drugs like Jasplakinolide and Latrunculin-B

2 MATERIALS & METHODS

Cell culture

Murine calvarial osteoblast cells (MC-3T3) were kindly provided from VU University Amsterdam from the department of Academic Centre for Dentistry Amsterdam (ACTA) and Hela cells were from the Leiden Institute of Physics at Leiden University. The MC-3t3 cells were cultured in T25 flasks with Gibco™ αMEM base media supplemented with 0.1% Sigma-Aldrich penicillin-streptomycin, 0.5% Gibco™ Fungizone and 10% Sigma-Aldrich fetal calf serum. The cells were stored in an incubator at 37°C in a humidified 5% CO2 atmosphere. At least once a week the media was changed and when the cells reached about 70% sub-confluency, they were passaged with Gibco™ Trypsin. The Hela cells were cultured in T25 flasks with Gibco™ DMEM base media supplemented with 0.1% Sigma-Aldrich penicillin and streptomycin, and 10% Sigma-Aldrich fetal calf serum. They were maintained in the same incubator at 37°C in a humidified 5% CO^2 atmosphere. Their media was also changed at least once a week and the cells were passaged with Trypsin when 70% sub-confluency was reached.

Equipment /data acquisition

Cells were passaged to an 8 well chamber slide from Ibidi two to seven days prior to the observation with the EVOS microscope. The EVOS microscope was equipped with a 40x (EVOS AMEP4983, numerical aperture = 0.65) and a 60x (Olympus N1507100, numerical aperture = 0.7) objective and the microscope camera has a frame rate of about 30 frames/s. It was placed in one of the gondolas in the Large Diameter Centrifuge (LDC) at ESA ESTEC which can create hypergravity conditions in the gondolas ranging between 1 and 20g (see Figure 1). Live feedback was provided to the control room from where the cells were observed while the LDC rotates. Brightfield and the GFP fluorescence were used to observe the cells. Videos of about 10s were recorded and saved per frame as raw tiff file to minimize data reduction by file compression. MATLAB was used to read in the files of the video and

compile it to one large tiff file. The image contrast of the individual frames was inverted such that dark particles appear as bright spots, which was necessary for later computation. Furthermore, videos made in hypergravity were corrected for drift via a MATLAB code.

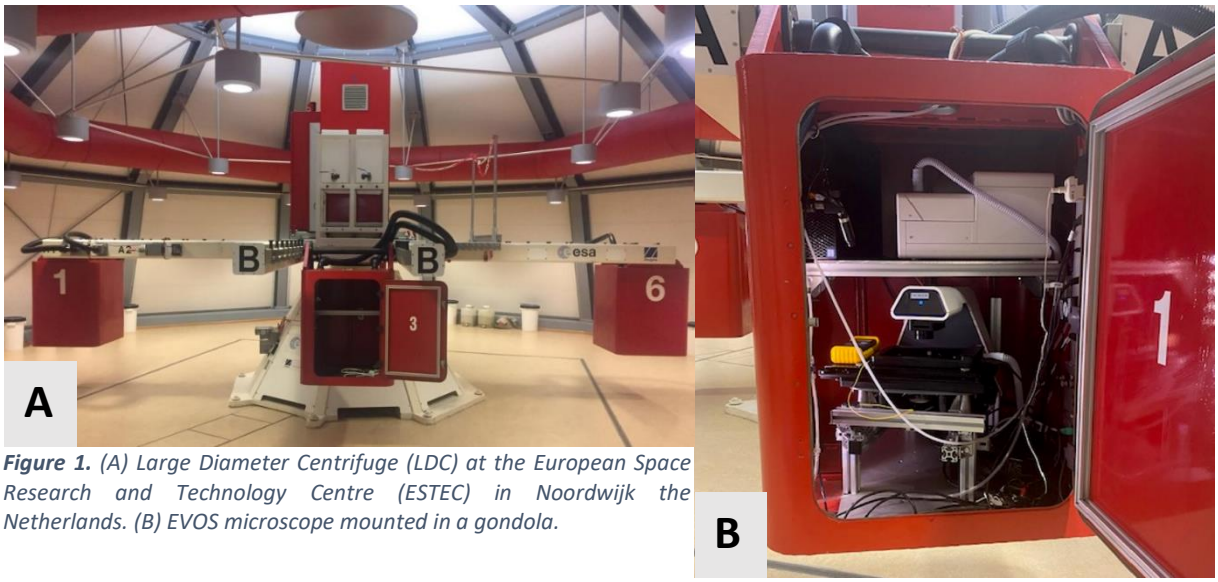

Figure 1. *(A) Large Diameter Centrifuge (LDC) at the European Space Research and Technology Centre (ESTEC) in Noordwijk the Netherlands. (B) EVOS microscope mounted in a gondola.*

Fluorescent staining of cells

Both MC-3T3 and Hela cells contain dark, unidentified, particles in Brightfield which were used for tracking. In an attempt to classify the particles, Invitrogen™ Mitotracker™ Green and Sigma-Aldrich Alizarin Red staining procedures were executed. MC-3T3 cells were passaged to four chambers in the 8 well chamber slide. After 6 days of culturing in the 8 well chamber slide, two chambers were stained with 50nM Mitotracker™ Green and allowed to set for 40 min. The other two chambers were dyed with 2% Sigma-Aldrich Alizarin Red stain and set for 10 min. The Hela cells were not stained due to time constraints of the thesis project.

Single-Particle Tracking software

To track particles in the cell the homemade Single-Particle Tracking software (SPT) made in MATLAB and created by the Schmidt lab at Leiden University was utilised[20].

Before evaluating the data files, several program settings were adjusted including the background mode, the threshold between background and signal, the Gaussian width, and the border of the image. All values were found via a trial-and-error approach for which several videos of endogenous particles in both Hela and MC-3T3, and the Invitrogen™ FluoSpheres® beads in sucrose solution (further explained in Validation) were analysed. Parameter values that found the most endogenous particles or FluoSpheres® beads and showed the least false positives were selected. The background mode ("Back" in Figure 2) describes the expected signal behaviour of the background. After testing various modes, mode 35, which describes a particular low-pass frequency filter, was found to be the best fit. The threshold between background and signal ("Threshold" in Figure 2) indicates the signal intensity

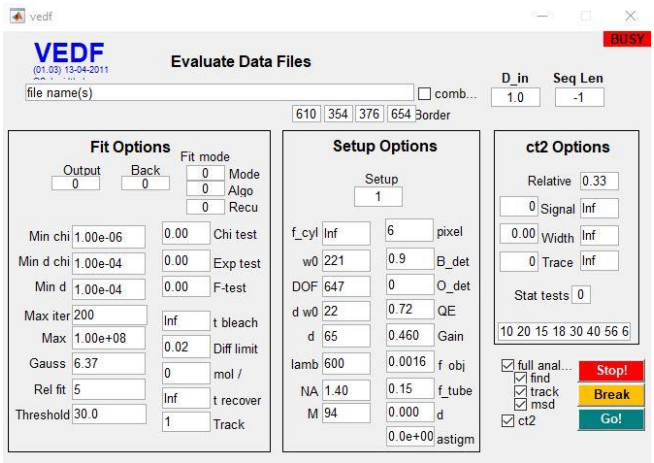

Figure 2. *Adjustable program settings of the Single-Particle Tracking software*

requirement for a signal to be perceived as signal and not as background. A threshold value of 50, which was the best fit for Hela cells, means that the signal intensity must be 50 times greater than the background signal to be classified as signal. For MC-3T3 a threshold of 20 resulted in the best fit, while a threshold of 30 worked best for the FluoSpheres® beads. The Gaussian width ("Gaus" in Figure 2) is the width of the Gaussian in pixels that is fitted on the intensity peaks of the image. It was found that a smaller Gaussian width was better as there was less chance of overshooting the intensity peak. However, the width was not allowed to be too small as this can result in finding a local maximum. The best fit for Hela and MC-3T3 cells was found for a Gaussian width of 5, while for the FluoSpheres® beads the default setting of 6.37 pixels performed better. The border of the video was determined uniquely for each video depending on the location of interest. For the cells, the location of interest were the endogenous particles, which only made up a small part of the image. Analysing only the area of interest significantly reduced the computational load, which could lead to time savings of several hours. The border value indicates the number of pixels removed from the left border, the right border, the top border, and the lower border of the image. Other parameters seen in Figure 2 that were not adjusted were found to have little effect or performed best at default settings.

After setting the software parameters, the recording was evaluated frame by frame which yielded the positions of the particles. For each frame the background signal was determined which is approximated with the anticipated background signal given in the settings. The program then scans the image for intensity peaks. These peaks are created by the photons from the sample striking the detection plane of the microscope. For every particle the signal was analysed and fitted to a nonlinear least-squares fit of a two-dimensional Gaussian for which the initial values of the width and intensity are given in the settings (see Figure 3).

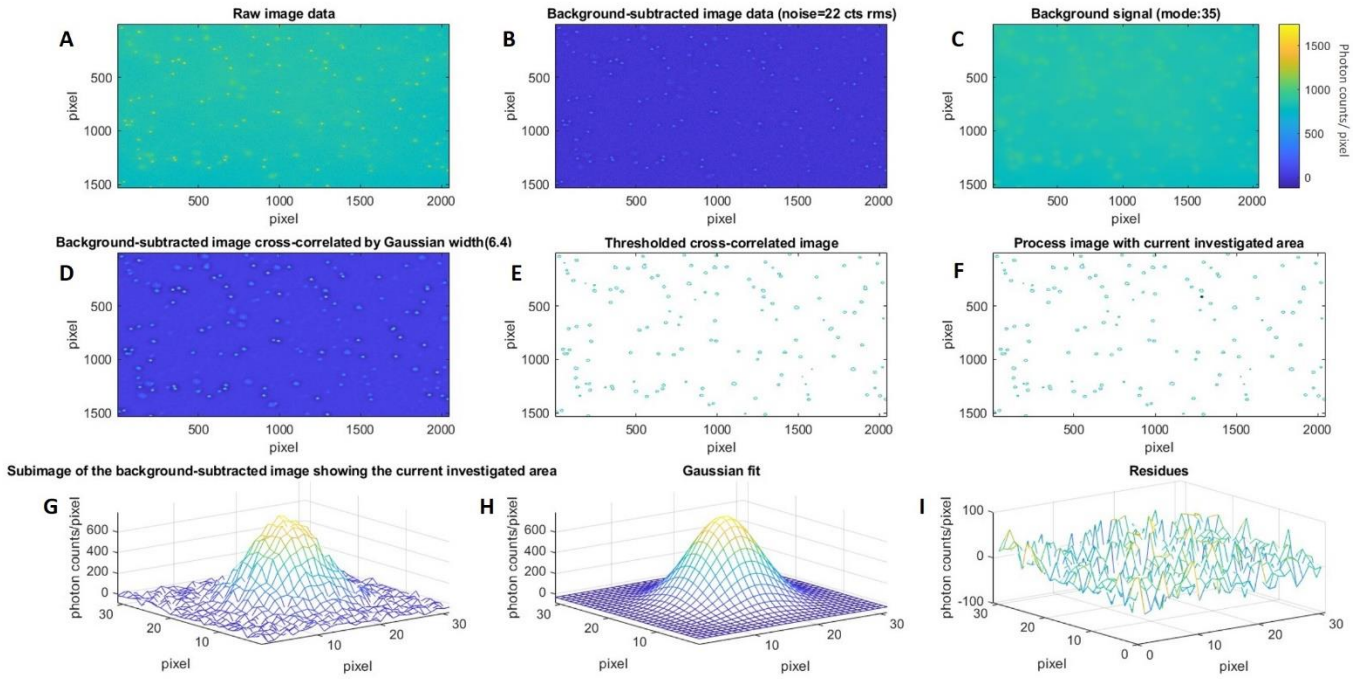

Figure 3. *The Single-Particle Tracking software fitting a nonlinear least-squares fit of a two-dimensional Gaussian on one of the signal peaks of the image. The colour coding for A, B, C, D, G, H and I is provided in figure C. (A) Raw image data: the image of the investigated frame displaying the pixel intensities . (B) Background-subtracted image data: the signal from the background is subtracted from the raw image data, the residual noise is 28 cts rms. (C) Background signal: the signal of the background with the selected background mode given in the SPT parameters. (D) Background-subtracted image cross-correlated by a Gaussian of width 6.4 pixel. (E) Thresholded cross-correlated image. (F) Process image with current investigated area: indicates the current signal (indicated in blue) that is tested if it complies with the set threshold value given in the SPT parameters. (G) Subimage of the background-subtracted image showing the current investigating area. (H) Gaussian fit: the nonlinear least-squares fit of a two-dimensional Gaussian fitted to the subimage shown in G. (I) Residues: the remaining signal of G after subtracting the Gaussian-fitted signal in H.*

The fit yielded the xy-position, width, and signal of all particles and for each frame of the recording. The xy-position determined by the mean of the Gaussian function, was determined on sub-pixel level. The positional accuracy, the standard error (SE), provides the positional error and was calculated with[25]:

$$\mathrm{SE} = \frac{\sigma}{\sqrt{n}} \ (Bobroff) \qquad \textit{(Equation 1)}$$

where n are the number of observed photons and σ the standard deviation of the Gaussian function. The probability of the positional error for all particles is given as output by SPT (see Figure 4).

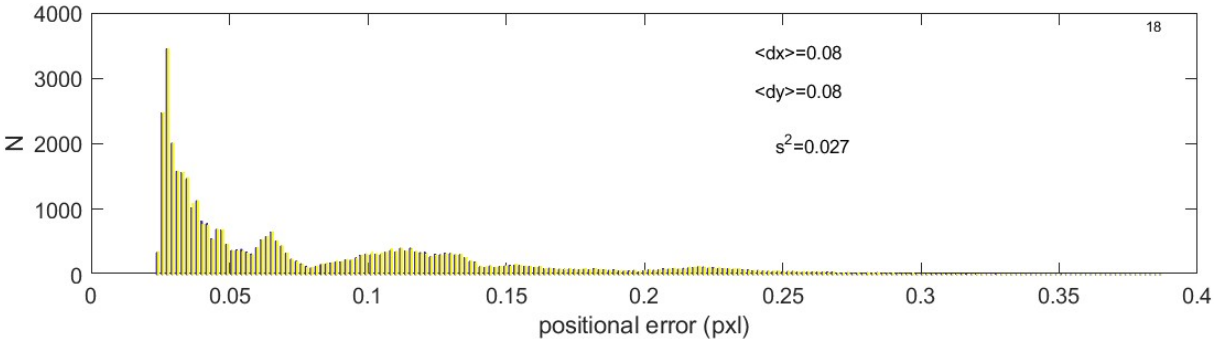

Figure 4. *An example of the probability of the positional error calculated by the Single Particle Tracking software. This figure displays the positional error in pixel (s^2) of FluoSpheres® in 60% sucrose solution at 20.7 °C in 1g with background = 35, threshold =30, and Gaussian width = 6.67. dx and dy are the errors in x and y direction and are described by a normal distribution. Assuming dx=dy the total squared distance in 2D to the true position is $s^2 = 4\,dx^2$. Number of particles = 432. 1 pixel = 0.080 µm.*

From the particle's observed width, the size of the particle can be estimated by:

$$w_{particle} = \sqrt{(w_{observed})^2 - (w_0)^2} \qquad \textit{(Equation 2)}$$

In which, w_0 , denotes the width of the point-spread function of the microscope which depends on the wavelength and Numerical Aperture of the objective as described by:

$$w_0 = \frac{\lambda^2}{2NA} \qquad \textit{(Equation 3)}$$

A wavelength of 550 nm is presumed such that $w_0 = 0.216\ \mu m$ for 60x objective and $w_0 = 0.233\ \mu m$ for the 40x objective. Again, the probability of the width for all particles is given as output by SPT (see Figure 5).

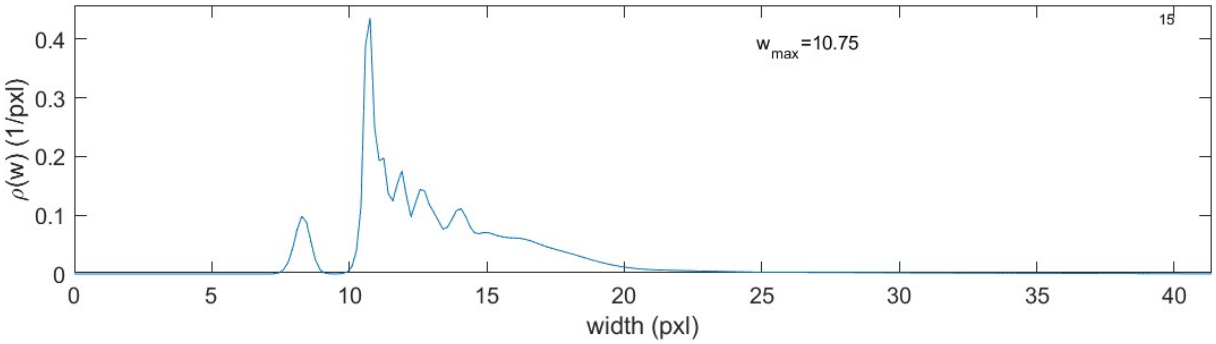

Figure 5*. An example of the probability of the observed particle's width calculated by the Single Particle Tracking software. This figure displays the probability of the observed particle's width in pixel for FluoSpheres® in 60% sucrose solution at 20.7 °C in 1g with background = 35, threshold =30, and Gaussian width = 6.67. w_{max} indicates the highest probability for the particle's width in pixel. Number of particles = 432. 1 pixel = 0.080 µm.*

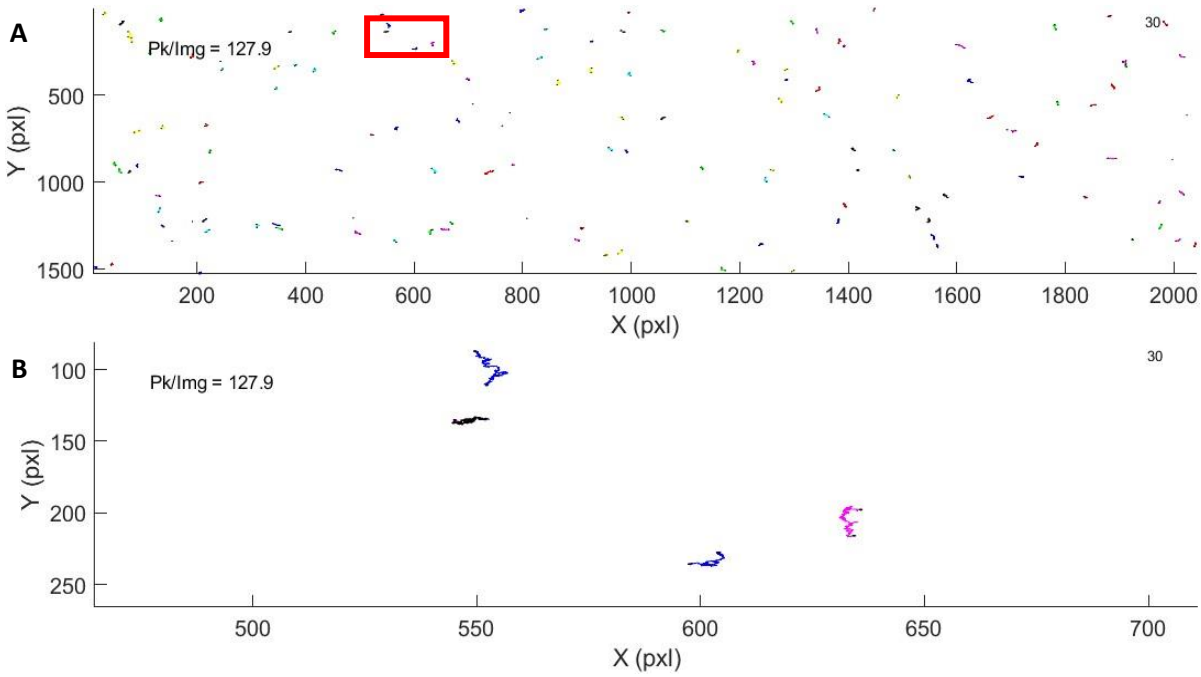

Figure 6. *An example of the trajectories of the particles in a recording calculated by the Single Particle Tracking software. This figure displays the trajectories in pixel of FluoSpheres® in 60% sucrose solution at 20.7 °C in 1g with background = 35, threshold =30, and Gaussian width = 6.67. (A) Full image and all trajectories. (B) Zoom in of the trajectories inside the red rectangle in A. Number of particles = 432. 1 pixel = 0.080 µm.*

After determining the positions of the particles, the frames are correlated with each other to determine the two-dimensional trajectory of each particle (see Figure 6).
Knowing the measured positions of all the observed particles over time (r_i), allows to calculate the Mean Square Displacement (MSD) for the time lag n between image i and i+n:

$$MSD = \frac{1}{N-n}\sum_{i=1}^{N-n}(r_{i+n} - r_i)^2 \qquad \textit{(Equation 4)}$$

The MSD is plotted against time lag (see Figure 7). The plot shows the travelled squared distance at a certain time. For example, the MSD at a time lag of 50 frames is the travelled squared distance between frame 1 and frame 50 of the video.

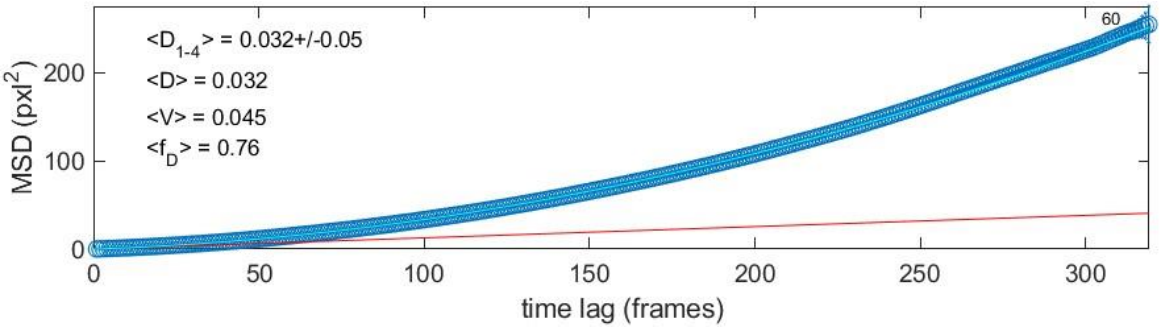

Figure 7. *An example of the MSD of the particles in a recording calculated by the Single Particle Tracking software. This figure displays the MSD in pixel² for FluoSpheres® in 60% sucrose solution at 20.7 °C in 1g with background = 35, threshold =30, and Gaussian width = 6.67. D is the estimated diffusion coefficient in pixel²/frame, V the velocity coefficient in pixel/frame, $D_{1\text{-}4}$ is the diffusion coefficient in pixel²/frame calculated for only the first 4 frames of the video, and f_d the fraction of diffusion compared to velocity calculated for the first 10 frames of the video. Number of particles = 432. 1 pixel = 0.080 µm.*

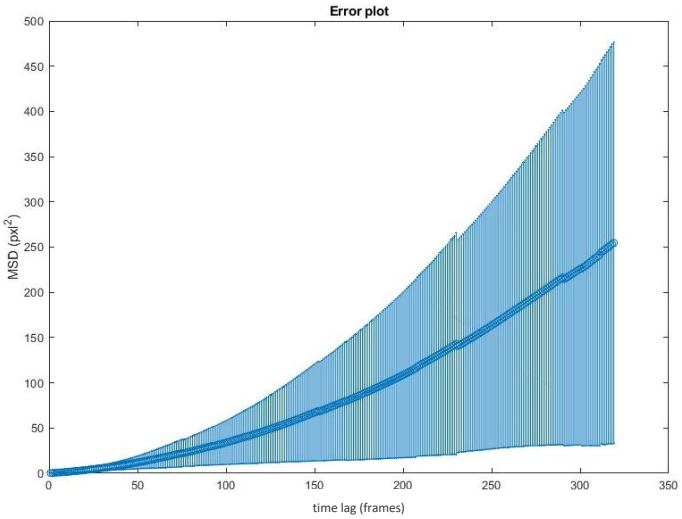

Figure 8. *The error plot of the MSD for the particles in a recording calculated by the Single Particle Tracking software. The error plot here displays the error in MSD over time lag for Figure 7 which is for FluoSpheres® in 60% sucrose solution at 20.7 °C in 1g with background = 35, threshold =30, and Gaussian width = 6.67. More uncertainties in MSD arise with increasing time lag. Number of particles = 432. 1 pixel = 0.080 µm.*

Naturally, with more time between frames, more uncertainties in MSD arise since less datapoints are averaged, and therefore the error increases with time lag (see Figure 8).

The SPT analysis used a model that allows for three processes to contribute to the MSD[26]. The term $4\sigma^2$ is included for the offset due to accuracy of the position determination caused by the precision of the microscope. Furthermore, the linear diffusion in two-dimensional space is incorporated with $4Dt$. Finally, to account for directed transport the function also contains the term and the final term $(Vt)^2$, which result in the equation:

$$MSD = 4\sigma^2 + 4Dt + (Vt)^2 \qquad \textit{(Equation 5)}$$

Optimising the SPT program for endogenous particles in Hela and MC-3T3 cells

The SPT program is created for single molecule tracking and required optimalisation to be applied for tracking particles in a cell. First a threshold was set for the minimum and maximum allowed values of the MSD. If a particle has a maximum MSD of less than 0.5 pixels^2 it is assumed to be static. Particles with an MSD over a 1000 pixels^2 are likely to show primarily directed transport and are discarded as well. A particle was also required to have at least three data points as any less datapoints do not allow for an accurate fitting of a function. In addition, a time lag of at least 15 frames (which is about 0.5s) is required to exclude brief, chaotic signals which usually terminate below 15 frames.

The first x-and y-coordinate of each optimised point was plotted in the first image of the tiff file to verify if the optimised points correspond to the appropriate tracking particles (see Figure 11b). Furthermore, this setup allowed to optimise the settings given by SPT in a trial-and-error approach. Moreover, this setup enabled the discovery of another problem. Occasionally, SPT loses a particle and then relocates it again due to a dip in intensity or a sudden jump in MSD, amongst other things. This phenomenon results in two close-proximity particles, while only one particle exists. To counteract this problem an additional boundary condition was set in which the distance between two optimised points cannot be less than 10 pixels in radius. If this requirement was not met, the particle with the longest time lag was selected and the other discarded.

Finally, during trials in de LDC it became apparent that the centrifuge induces a lot of vibrations. Without interference this results in limited observed time lag for all optimised particles. Before running SPT, the videos were stabilized with a MATLAB code that determines and adjusts for the drift in x-and y-direction by full-image correlation.

MSD calculation selection

As previously mentioned, the SPT program uses (Equation 5, which assumes diffusion and directed movement. However, multiple MSD functions exist for various diffusion behaviour. Figure 9 shows a variety of diffusion behaviour along with their function. To determine the appropriate diffusion function, the MSD data is plotted in a logarithmic scale plot and fitted to $y = \alpha x + b$. If α =1 there is pure diffusion which for a two-dimensional space can be described by $4Dt$. If α is larger than 1, superdiffusion is observed for which the function contains, beside the normal diffusion term, also a term describing directed transport. The SPT program assumes this type of diffusion as molecules often display active transport as well. For α<1, subdiffusion is observed. Confined or corralled diffusion is a type of subdiffusion for which after a certain time lag the MSD does not increase anymore with increasing time lag. Reasons for this type of behaviour include caged particles. Finally, anomalous diffusion describes a non-linear behaviour for which diffusion is suppressed. This behaviour has been observed before in Hela cells[27,28]. The scaling exponents do seem to vary from sub-diffusion to super-diffusion depending on cell type[29], and also on their environment like temperature and ATP availability[30].

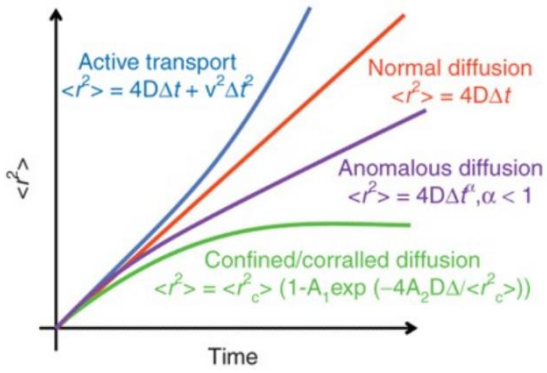

***Figure 9**. Time scale MSD over time lag graph displaying several types of diffusion behaviour along with their function. Taken from Ruthardt N. et al. (2011)* [1]

The type of diffusion is determined for each video by fitting the MSD data on a logarithmic scale and fitting the function $y = \alpha x + b$. For anomalous diffusion instead of using the function given in Figure 9 we apply the following function as described by Kusumi et al. (2013)[26] and adjust by Lommerse et al. (2005)[31] to:

$$r^2(t_{lag}) = (4\sigma)^2 + \frac{L^2}{3} \cdot [\, 1 - e^{\frac{-12Dt_{lag}}{L^2}} \,] \qquad \textit{(Equation 6)}$$

The function describes Brownian diffusion of a particle confined within a square with length L that cannot move outside the impermeable, reflecting barrier during the observation period[26,31]. Although the function $MSD = 4Dt^{\alpha}$ can be applied to describe anomalous diffusion, the unit of the diffusion (D) is altered and becomes time-dependent, thereby complicating further calculations.

Viscosity determination

Both (Equation 5 and (Equation 6 can be applied for Brownian diffusion. It is assumed that the solution behaves as a purely viscous fluid (Newtonian) such that the obtained diffusion coefficient can be used to calculate the viscosity with the Stokes-Einstein equation for a spherical object[32]:

$$D = \frac{k_b T}{\eta 6\pi r} \qquad \textit{(Equation 7)}$$

Here, D is the diffusion coefficient, k_b the Boltzman constant, T the temperature, η the viscosity, and r the radius of the sphere. The term $k_b T$ describes thermal energy, and $6\pi r$ is the frictional coefficient a particle experiences due to the random forces created by the thermal energy. The surrounding solvent molecules collide with the particle and as a response alter the particle's position[19]. The Stokes-Einstein equation assumes that the solution is incompressible, has a low Reynolds number and that the local environment around the particle is isotropic. Furthermore,

inertial effects are also neglected as they become primarily substantial at microsecond time scales[33] and at sub-femtosecond in solution (personal communication Prof. dr. Thomas Schmidt).
All the aforementioned assumptions are valid for the validation test outlined in the following paragraph for which spherical probes submerged in a sucrose solution exhibit pure Brownian motion. However, for the trials with cells, it is rather an oversimplification. Particles in a living cell are not expected to have pure Brownian diffusion. The cells have cytoskeletons, and the cytoplasm contains numerous proteins and organelles which collectively represent a complex system. The tracking particles are estimated to be larger than the average pore size of the cytoskeleton meshwork which is between 20 and 40 nm[34]. Therefore, the particles will not move freely through the network but will encounter resistance of the cytoskeleton, which contributes to the anomalous diffusion and hence the cytoskeleton will also strongly contribute to, if not dominate, the perceived viscosity[27]. Furthermore, since the tracking particles have not been identified, it is uncertain whether they are truly spherical. Although the particles occur spherical in the images, the diffraction limit may cause them to appear circular when they are not.
By evaluating only a small time lag (1-10), which is about 0.3s, the time-dependent effect of viscoelastic behaviour is minimized and aids to approach $\alpha = 1$. Figure 27 shows that even for a small time lag, α is smaller than 1 which indicates that in a short time span the particle can still encounter resistance from the cytoskeleton or other structures. As the particles identity is unknown, it is unclear if the particles are connected to each other or other cell structures. Although quite some assumptions are made which oversimplify the complex nature of the cells and therefore limit the outcome in providing an exact viscosity, it still allows to answer the main objective of this study which confronts if viscosity changes at all in hypergravity.

Validation
To evaluate the described system, experiments were conducted in which the size of the particles and the viscosity of the solution were known in advance. Invitrogen™ FluoSpheres® carboxylate yellow-green 1.0 µm (with an actual size of 1.1 µm, displayed on the container for Lot:1109819) were kindly provided by the Koenderink lab from the department of Bionanoscience at Delft University of Technology. A solution of 60% and 30% sucrose dissolved in milli-Q was made. To assist the dissolving of the sucrose the solution was slightly heated to 35◦C while stirring. The lid was covered to minimize evaporation leaving the flask, which would otherwise result in an increase in the concentration of sucrose. The solution was allowed to cool down to room temperature before continuing experiments. The vial with FluoSpheres® was placed in an ultrasonic bath for 1 minute to reduce cluster formation. In 1 ml of sucrose solution 10 µL of Fluospheres® was injected. The solution was vortexed for 30s to create a homogeneous solution. On an 8-well plate, 2 wells were loaded with 0.3µL of the solution per well. One was loaded with 60% sucrose and the other with 30% sucrose. The plate was mounted into the EVOS microscope in the LDC. Per gravity level, 10 videos were made for both concentrations of sucrose. For the 60% sucrose solution gravity levels 1,2,4,6,8 and 10g were tested. For the 30% sucrose solution the same gravity levels were measured except from the 10g as the vibration of the particles was too severe to make proper videos.

3 RESULTS

During the setup of the project, it was planned that the MC-3T3 cell would be used as the test subject. Although cell culture started off well for the first month, the condition of the cells appeared to worsen over time. Several cell cultures were tested in which lower passage numbers and different concentrations of penicillin-streptomycin were tested. At some point, contamination was suspected. Every lab tool, including the incubator, was thoroughly cleaned, the condition of the chemicals was

checked, and the fetal calf serum was replaced out of precaution, but the condition of the cells remained poor. An Invitrogen™ Hoechst stain was performed on the cells which can indicate Mycoplasma contamination. However, the stain did not show any contamination. The source of the problem was not found, and with the limited time of the project, another cell type was selected. Hela cells were chosen as they were kindly gifted from the Schmidt lab and are known to be a robust kind of cell.

Alizarin Red staining

The next step was to identify the tracking particles. Literature and various lab technicians were consulted, but no clear or conclusive answer was found. I suspected that the particles might be calcium deposits as the cells are pre-osteoblast and could potentially be maturing. An Alizarin Red stain allows to identify calcium deposits. However, the staining procedure did not result in stained particles as can be seen in Figure 10. Therefore, it is unlikely that the observed dark particles are calcium deposits. A close-up of the unidentified particles is also provided in Figure 10. The stain was not tested on Hela cells due to limited time of the thesis project, and because it is less likely that Hela cells contain calcium deposits as they are not pre-osteoblasts.

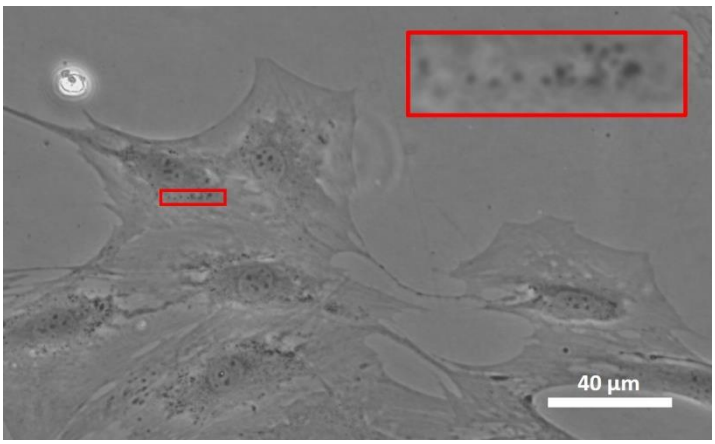

***Figure 10**. MC-3T3 cells stained with 2% Alizarin Red at 40x zoom. The rectangle in red shows a zoom-in of the endogenous particles.*

Comparison Brightfield and GFP

Another stain that was applied to identify the particles was Mitotracker™ Green. The fluorescent label stains mitochondrial proteins by binding to free thiol groups of cysteine residues[35]. The stain with Mitotracker™ Green was successful and resulted in stained spots as can be seen in Figure 12a. The size of these dots does not seem to correspond with the size of the unidentified particles. Furthermore, the dimensions of the fluorescent particles appear to vary within the cell as well. Therefore, I suspect that the unidentified particles are not mitochondria. Mitotracker™ Green staining was not applied to Hela cells. The condition of the MC-3T3 cells did not reveal any defects yet in this moment of time. Due to the limited time of the thesis, it was not possible to apply the Mitotracker™ Green staining to Hela cells.

Since the unidentified and MitoTracker-Green-stained particles do not appear to be the same, the GFP and the Brightfield approach were compared to determine what would yield a better method for tracking particles.

After running the optimised SPT, the MSD of the found particles for GFP is shown in Figure 11b and the MSD in Brightfield in Figure 12b. The particles in Brightfield seem have a higher mobility than the stained particles in GFP. In fact, the minimum scale of MSD threshold had to be adjusted to 0.1 pixel^2 to prevent all particles from being discarded due to the set MSD threshold. Particles with a low mobility are not prefered as the noise will be more dominant in the particle's signal. This is confirmed in the MSD plots of the fluorescent particles as the lines appear more chaotic compared to the lines of the MSD performed in Brightfield. Furthermore, it seems that more particles are identified and pass the optimalisation criteria for Brightfield when comparing Figure 11c and Figure 12c. Hence, from these results the Brightfield approach was selected for furter experiments.

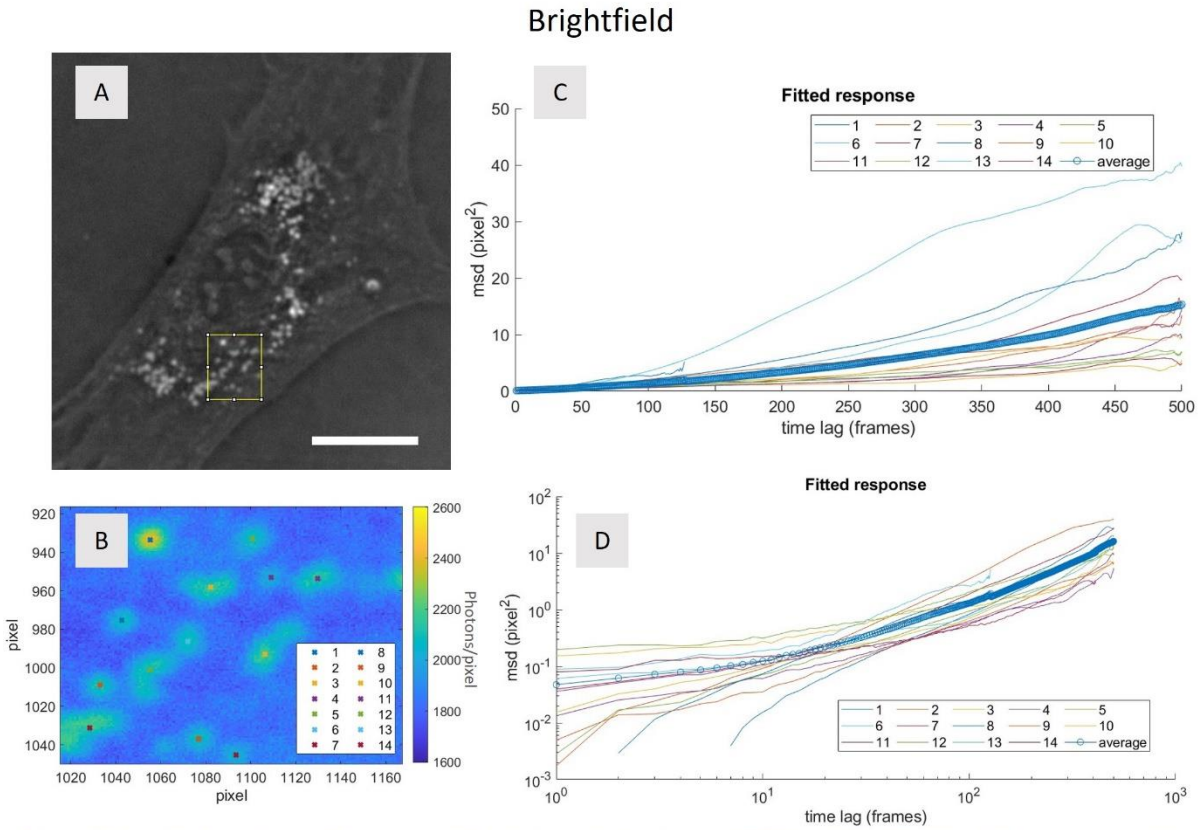

Figure 11. *Brightfield analysis at 60x zoom for MC-3t3 cells at 21 °C in 1g for BORDER = [1020, 906, 916, 466], background = 35, threshold =20, and Gaussian width = 5. (A) First contrast inverted image of the recording showing the selected area for analysis in yellow. (B) First image of the recording after analysis showing the selected area with all the particles for which the particles that passed the optimalisation criteria are indicated with a cross. (C) MSD over time lag for all the optimised particles and the average of all the MSDs. (D) Logarithmic scale plot of MSD over time lag for all the optimised particles and the average of all the MSDs. 1 pixel = 0.080 µm.*

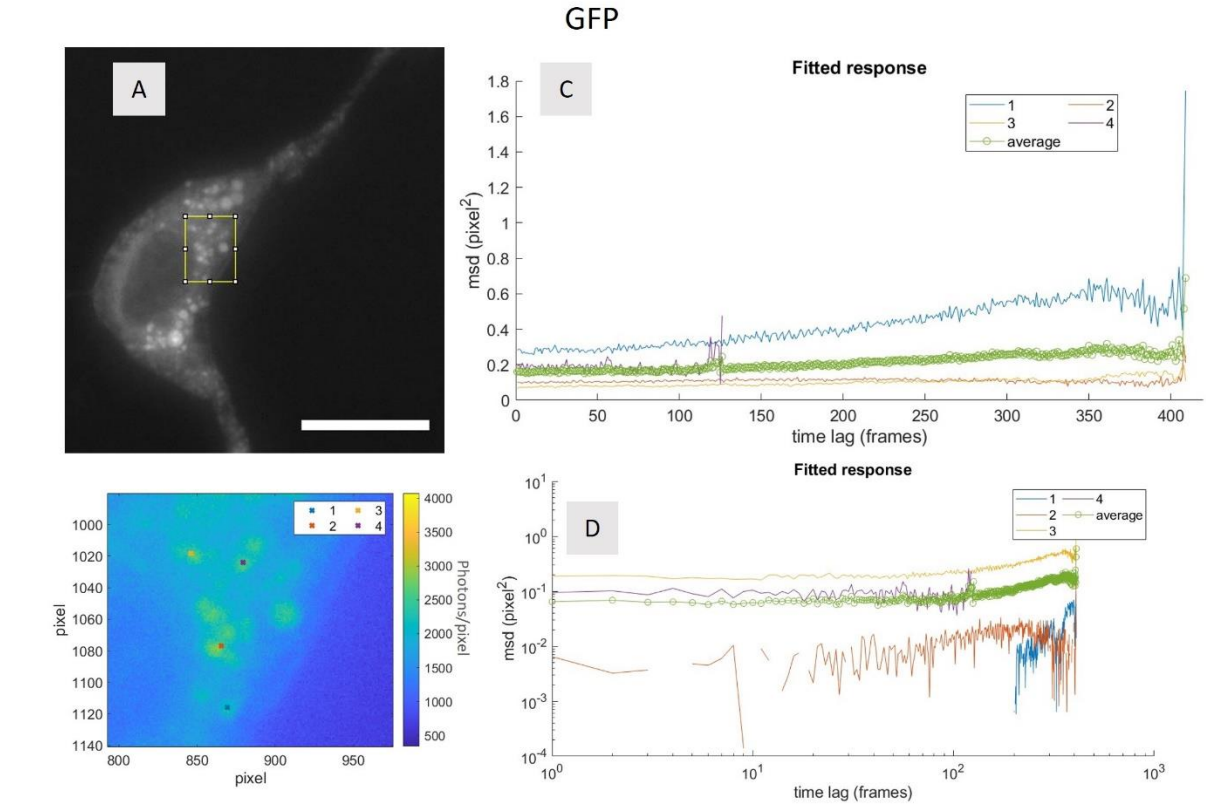

Figure 12. *MitoTracker™ Green analysis at 60x zoom for MC-3T3 cells at 21 °C in 1g for BORDER = [830, 1112, 992, 414], background = 35, threshold =20, and Gaussian width = 5. (A) First image of the recording showing the selected area for analysis in yellow. (B) First image of the recording after analysis showing the selected area with all the particles for which the particles that passed the optimalisation criteria are indicated with a cross. (C) MSD over time lag for all the optimised particles and the average of all the MSD. (D) Logarithmic scale plot of MSD over time lag for all the optimised particles and the average of all the MSD. 1 pixel = 0.080 µm.*

LDC vibration

The 0.050 mm dots on the Invitrogen™ EVOS™ Calibration Slide (see Figure 13) was used to investigated the vibrations of the centrifuge. The slide was mounted in the microscope and recordings were taken for 1g up to 20g in steps of 2g. The dot on the calibration slide was fixed, therefore it should not show any MSD aside from some noise caused by the accuracy of the microscope. Figure 14a shows the MSD plot for the 60x zoom objective at 4g and Figure 14b at 18g. Without any correction for the vibration the programm detects a significant MSD which seems to increase with g level. Furthermore, for 18g, the longest observed time lag is 11 frames. Figure 14c and Figure 14d show the MSD plot for the 60x zoom objective at 4 and 18g after applying the xy-drift correction MATLAB code. The programm managed to significantly reduce the observed MSD to noise level. The xy-drift correction was applied for furter experiments with increased g levels.

Figure 13. *0.050 mm diameter dot on the Invitrogen™ EVOS™ Calibration Slide at 60x zoom used to investigated the vibrations of the LDC and the effectiveness of the xy-drift correction.*

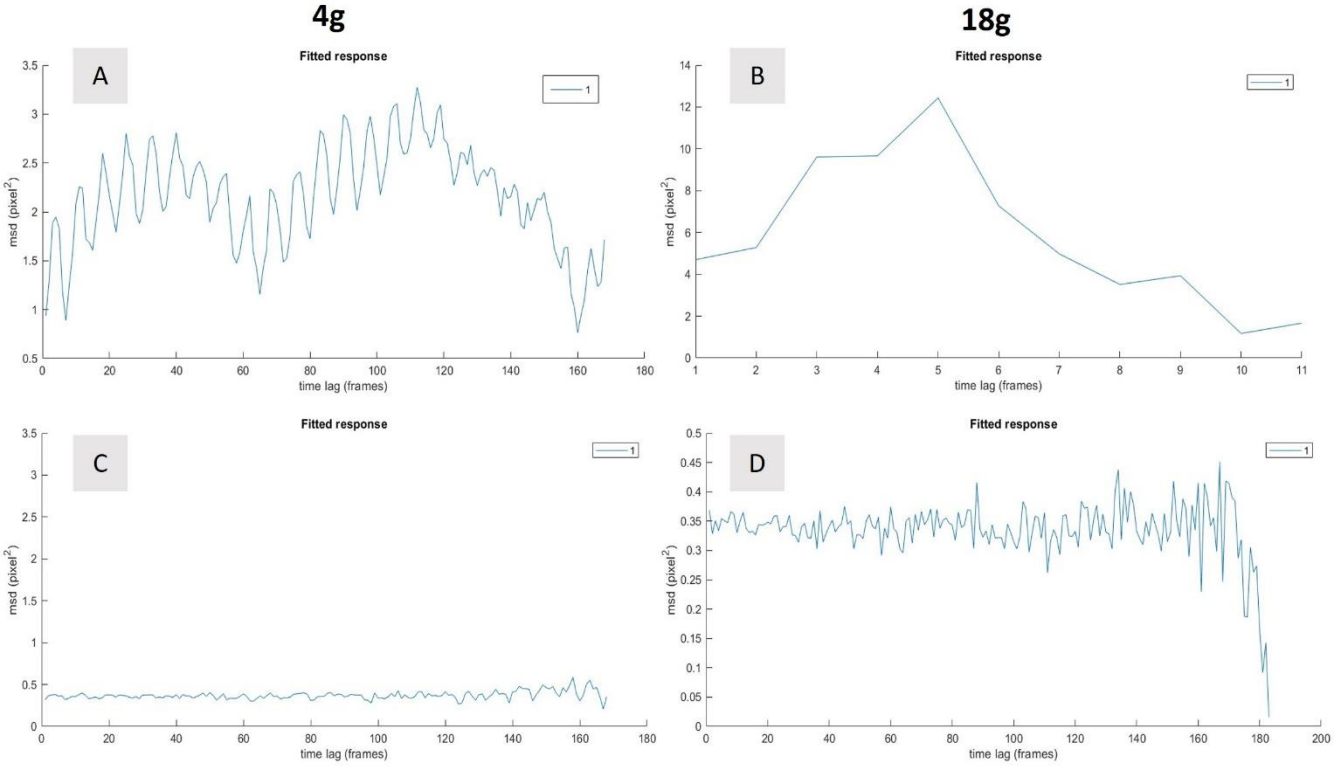

Figure 14. *Comparison of the MSDs before and after xy-drift correction for 4 and 18g. (A) MSD over time lag for the calibration slide at 60x zoom in 4g without xy-drift correction. (B) MSD over time lag for the calibration slide at 60x zoom in 18g without xy-drift correction. (C) MSD over time lag for the calibration slide at 60x zoom in 4g after applying xy-drift correction. (D) MSD over time lag for the calibration slide at 60x zoom in 18g after applying xy-drift correction.*

Validation test

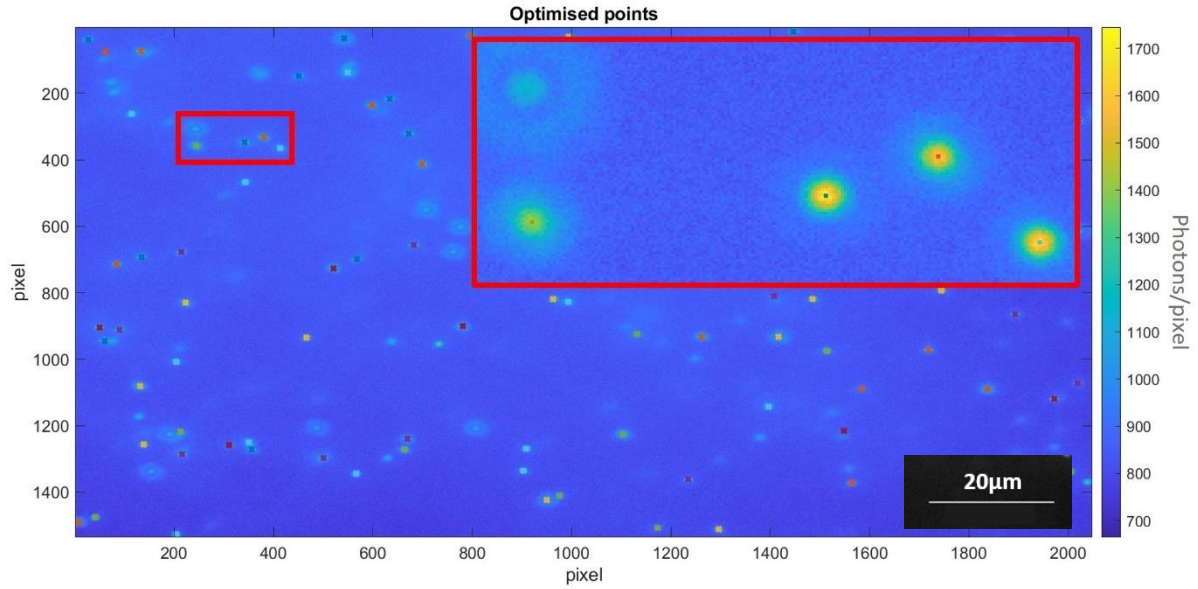

Figure 15. *Image of FluoSpheres® in 60% sucrose solution at 20.7 °C in 1g with background = 35, threshold =30, and Gaussian width = 6.67. Optimised particles are indicated with a cross. The rectangle in red shows a zoom-in of the particles. The particle in the top left corner of the zoom-in is too far out of focus and not selected as it failed the optimalisation criteria or the criteria set by SPT. 1 pixel= 0.080 µm.*

The SPT and optimalisation were able to identify most of the FluoSpheres® in the 60% sucrose solution as seen in Figure 15. Some particles have not been selected as they failed the optimalisation criteria or the criteria set by SPT.

The size for each of the optimised particles is calculated by SPT. A histogram of the size distribution is provided in Figure 16. The mean of the width of all the particles is 13.9 pixels. For the 60x zoom objective, 1 pixel is 0.080 µm. Converted to µm this results in 1.11 µm which is in line with the known value (1.1 µm) for the diameter of the FluoSpheres®. Some particles appear to have a slightly larger width. This could be caused by the probes being out of focus, as can be observed in Figure 15.

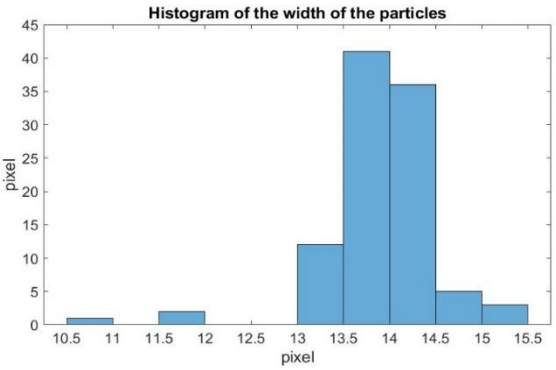

Figure 16. *Histogram of all the widths for the optimised particles in the recording of FluoSpheres® in 60% sucrose solution at 20.7 °C in 1g with background = 35, threshold =30, and Gaussian width = 6.67. 1 pixel = 0.080 µm.*

In the next step, the MSDs for all optimised points were plotted on a logarithmic scale (see Figure 18). The average of all points and the fitting to the function $y = \alpha x + b$ was also provided. The plot appears to have a slope of one, especially for the low numbers of time lag. Each line was individually fitted to $y = \alpha x + b$ and a histogram of the α distribution in given in Figure 17. The mean for α for all optimised particles is 1.03 and the standard deviation is 0.15. The solution is only sucrose with

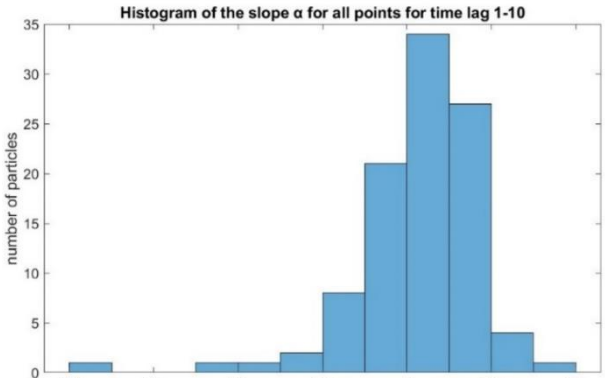

Figure 17. *Histogram of all the fitted α for the function y=αx+b for the optimised particles in the recording of FluoSpheres® in 60% sucrose solution at 20.7 °C in 1g with background = 35, threshold =30, and Gaussian width = 6.67*

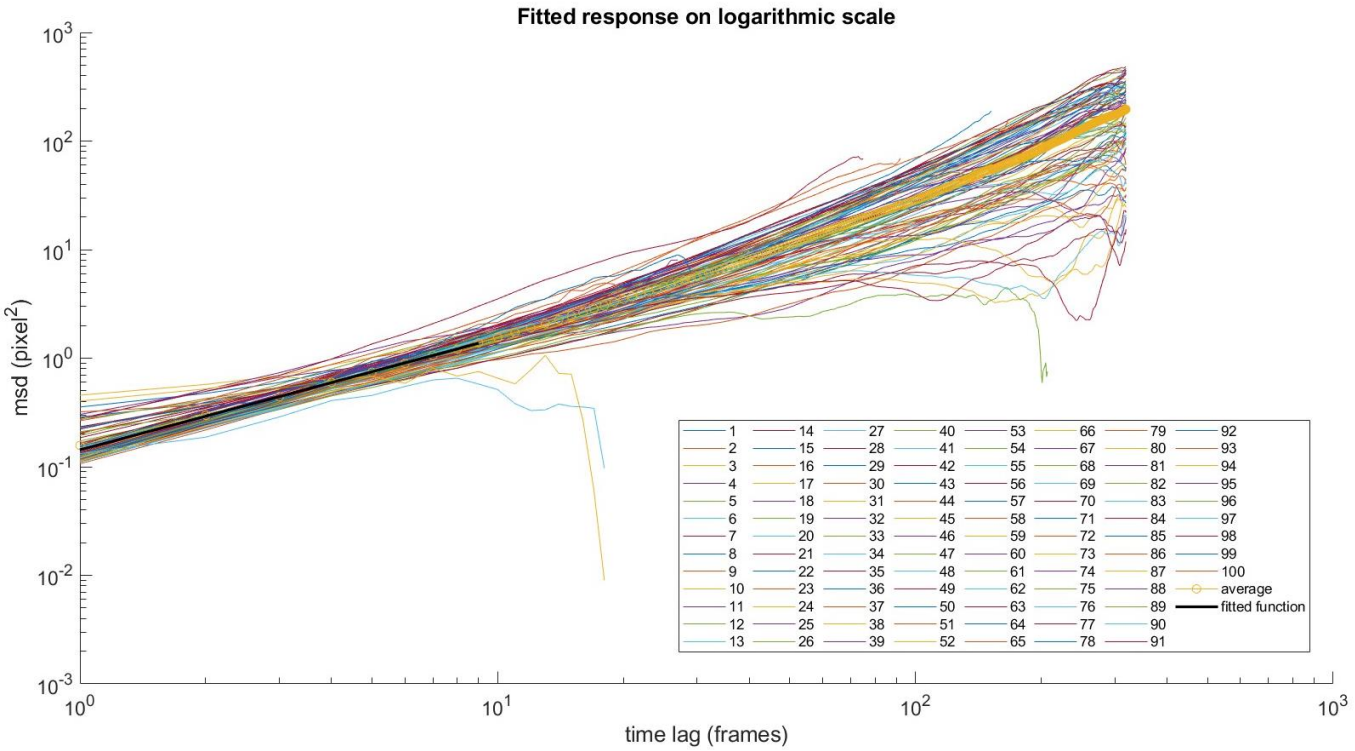

***Figure 18**. Logarithmic scale plot of the MSD over time lag for each optimised particle for the FluoSpheres in 60% sucrose solution at 20.7 °C in 1g with background = 35, threshold =30, and Gaussian width = 6.67. The average is defined as the sum of all the MSD values for the optimised particles at a certain time lag divided by the number of particles at that specific time frame. Each line in de plot is representing a single particle. Each line is individually fitted to y=αx+b and the average of all these fittings is displayed as "fitted function".*

probes and therefore should show only Brownian diffusion with α=1. Although 1.03 is close to 1, there appears to be a slight directed motion, while there should not. Upon further inspection of the videos, it seemed that the drift direction changed over time and that it was not uniform in the field of view. Furthermore, the magnitude of the drift appeared to increase in later videos. It was speculated that the light of the microscope induced heat, thereby creating local currents. To test this suggestion a thermometer was connected to a slide and the light was focused on the sensor of the thermometer as seen in Figure 19. The temperature measurements are provided in Table 1 for the 60x objective and in Table 2 for the 40x objective. Pure white light does not seem to affect the temperature much, but the GFP filter does show a significant increase in temperature. Illuminating the sensor for only 15s, which is the time required to focus on the sample and to record a video, resulted in 0.5 °C maximum temperature increase for the 60x objective and up to 1.4 °C for the 40x objective. Moreover, switching between objectives, especially without adjusting the brightness first, can results in an instantaneously change of several degrees Celsius. Furthermore, the temperature in the incubator also slowly rose while conveying the experiments. The start temperature in the incubator was 21.3°C and within 35 minutes increased to 21.8°C.

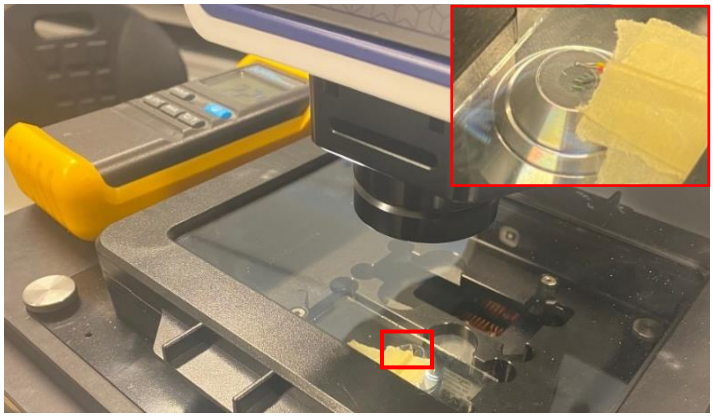

***Figure 19.** Arrangement to test the temperature induced by the light of the EVOS microscope. In the red rectangle a close-up of the temperature sensor above the objective.*

Table 1. Temperature measurement for the 60x objective for 15s illumination with pure white light and with a GFP filter for different brightness settings and distances to the slide (coarse).

	white		GFP filter	
	T_0 (°C)	**T_{15} (°C)**	**T_0 (°C)**	**T_{15} (°C)**
	Brightness = 0.010			
coarse = 393.7	21.3	21.4	21.3	21.9
coarse = 990.0	21.3	21.4	21.4	21.5
	Brightness = 0.00081			
coarse = 393.7	21.5	21.6	21.5	21.9
coarse = 990.0	21.6	21.6	21.6	21.6
	Brightness = 0.0048			
coarse = 393.7	21.9	21.9	21.8	22.3

Table 2. Temperature measurement for the 40x objective for 15s illumination with pure white light and with a GFP filter for different distances to the slide (coarse).

	white		GFP filter	
	T_0 (°C)	**T_{15} (°C)**	**T_0 (°C)**	**T_{15} (°C)**
	Brightness = 0.0048			
coarse = 397.2	21.9	21.9	21.9	23.1
coarse = 621	22.1	22.1	22.1	23.1
coarse = -202.2	22.2	22.2	22.2	23.6

To account for the additional drift seemingly created by the heat flows induced by the microscope, the MSD function of Equation 5 is used. The drift is captured in the velocity term such that the diffusion term remains unaffected. The MSDs for all optimised points against time lag are plotted in Figure 20.

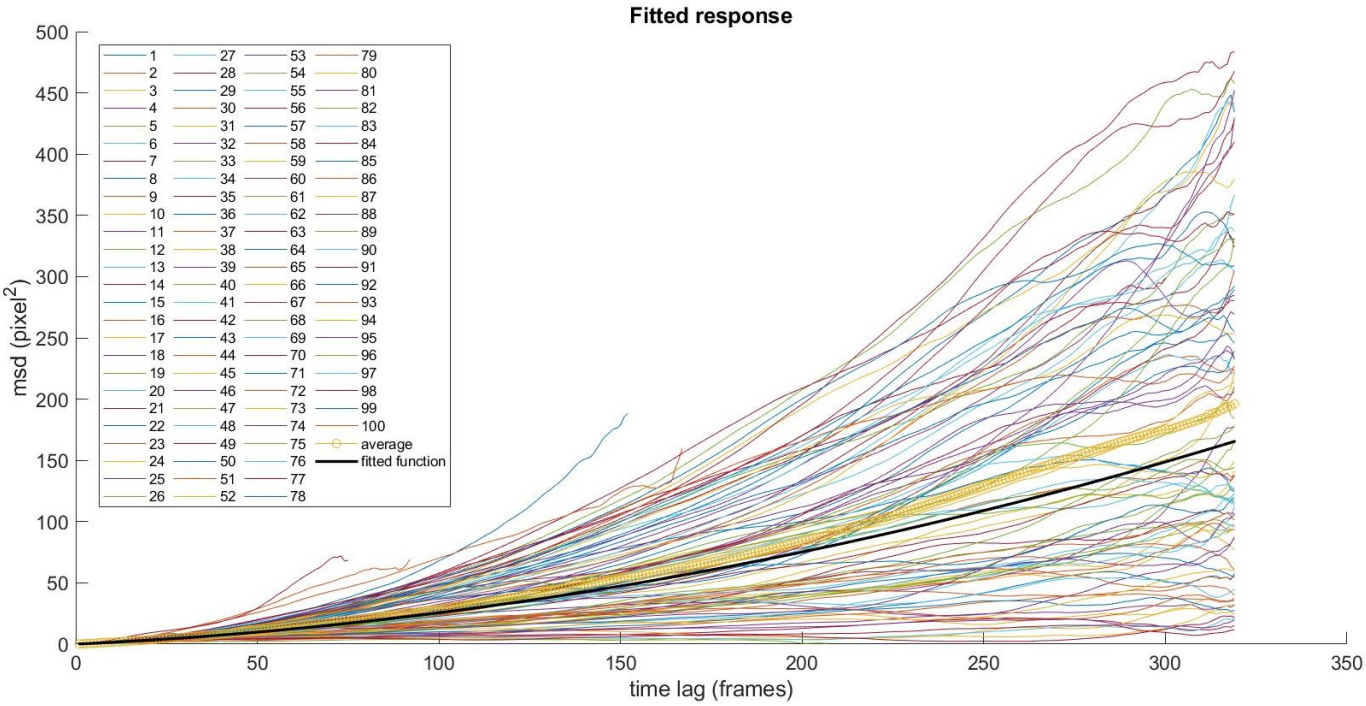

Figure 20. *Plot of the MSD over time lag for each optimised particle for the FluoSpheres® in 60% sucrose solution at 20.7 °C in 1g with background = 35, threshold =30, and Gaussian width = 6.67. The average is defined as the sum of all the MSD values for the optimised particles at a certain time lag divided by the number of particles at that specific time frame. Each line in de plot is representing a single particle. The fitted function is determined by fitting the function* $MSD= 4\sigma^2+4Dt+(Vt)^2$ *to each individual particle after which the mean of the D distribution and the V distribution is taken to create the fitted MSD function.*

Each particle is individually fitted to Equation 5 and a histogram of the distribution for the diffusion coefficient, the velocity coefficient, and the fraction of diffusion compared to velocity, are given in Figure 21, Figure 22 and Figure 23. The mean of the diffusion coefficient for FluoSpheres® in 60% sucrose solution at 20.7 °C is 0.0340 with a standard error of 0.0034 and the mean of the velocity coefficient is 0.0346 with a standard error of 0.0023. The means of the diffusion and velocity coefficient histograms were inserted in Equation 5 and plotted in Figure 20 as "fitted function". The fraction of diffusion, f_d, aids in determining the dominant behaviour in the sample. A f_d close to one indicates that diffusion is the leading behaviour in the sample. For a time lag of 10 for the FluoSpheres® in 60% sucrose solution at 20.7 °C the mean f_d is 0.7147 and the standard error is 0.0462. Hence, the major behaviour is caused by Brownian diffusion, which is to be expected as inherently the velocity coefficient becomes dominant at larger time lag.

In the final step, the mean diffusion coefficient, the temperature, and the mean width of the particles were inserted in the Stokes-Einstein equation (see *Equation 6*) to calculate the viscosity. The error in the viscosity will be predominantly determined by the error in the diffusion coefficient and the error in the width determination.

Hence, the following equation derived by a Taylor expansion is used to determine the error of viscosity: Here dD is the standard error for all the fitted D and

$$d\eta(D,r) = \sqrt{((\frac{dD}{D})^2 + (\frac{dr}{r})^2) * \eta^2} \qquad \textit{(Equation 8)}$$

dr is the mean of all the standard errors of the width. For the FluoSpheres® in 60% sucrose solution at 20.7 °C in 1g this gave 59.48 +/- 5.96 mPa*s. This is in line with literature for which 60% sucrose solution at 20.7 °C gives a viscosity[36] of 56.16 mPa*s or a viscosity[37] of 54.96 mPa*s.

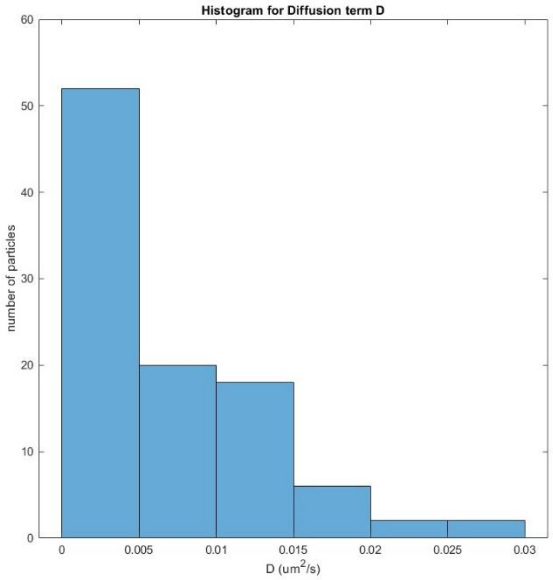

Figure 21. *Histogram of the fitted diffusion coefficient D for all optimised particles for the function MSD= 4σ2+4Dt+(Vt)2 in the recording of FluoSpheres® in 60% sucrose solution at 20.7 °C in 1g with background = 35, threshold =30, and Gaussian width = 6.67*

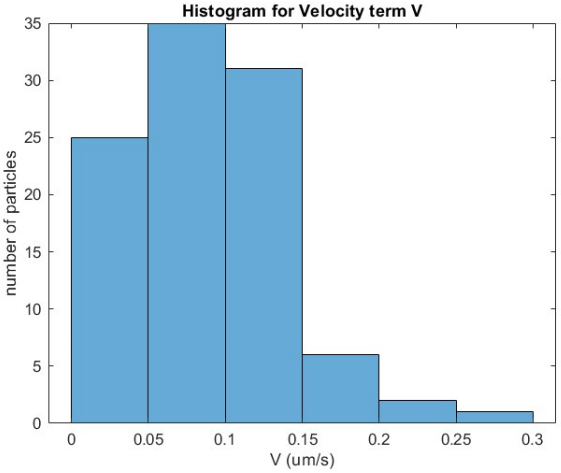

Figure 22*. Histogram of the fitted velocity coefficient V for all optimised particles for the function MSD= 4σ2+4Dt+(Vt)2 in the recording of FluoSpheres® in 60% sucrose solution at 20.7 °C in 1g with background = 35, threshold =30, and Gaussian width = 6.67*

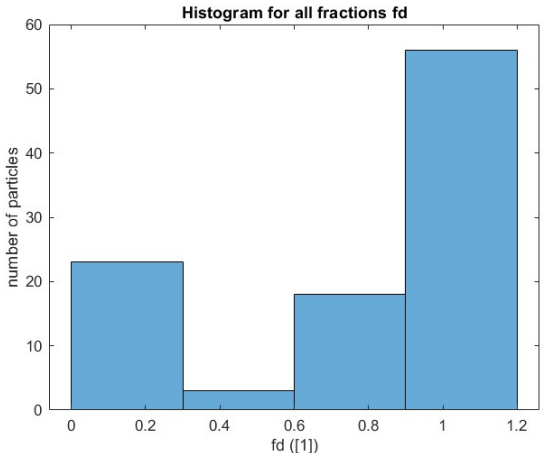

Figure 23*. Histogram of diffusion fraction fd for the first 10 frames of the video, calculated with the fitted diffusion coefficient and velocity coefficient for all optimised particles for the function MSD= 4σ2+4Dt+(Vt)2 in the recording of FluoSpheres® in 60% sucrose solution at 20.7 °C in 1g with background = 35, threshold =30, and Gaussian width = 6.67*

For both 60% sucrose and 30% sucrose solution three videos in 1g were analysed and the results are given in Table 3. The mean of the viscosity of 60% sucrose solution is close to the expected value. The logarithmic exponent is 1 and thus represents Brownian diffusion. The mean of the particle size appears to be slightly larger than the expected 13.75 pixels. Furthermore, the particle size seems to increase slightly for later videos. This could be a result of more pronounced heat flows for which particles become out of focus during the recording as they move along the heat current in z-direction. For the 30% sucrose solution, a mean viscosity of 4.82 mPa*s was found, while in literature[36,37] the viscosity of 30% sucrose at 22.2 °C is 2.977 mPa*s or 2.964 mPa*s. It is suspected that an inaccuracy during the preparation of the solution caused a slight change in sucrose concentration. Again, the mean of the calculated particle size is slightly higher than the actual size, which is predicted to be caused by blurred particles in the image.

Table 3. *Calculated viscosities, logarithmic exponent α and particle width for recordings of FluoSpheres® in 60% sucrose solution at 20.7 °C in 1g and in 30% sucrose solution at 22.2 °C in 1g.*

	60% sucrose solution		
	Viscosity (mPa*s)	**α**	**Particle width (pixel)**
video 1	59.48	1.03	13.89
video 2	45.64	1.01	14.37
video 3	54.21	0.97	15.27
mean	53.11 +/- 4.0	1.00 +/- 0.0176	14.51 +/- 0.404
	30% sucrose solution		
video 1	4.08	1.06	13.97
video 2	4.67	1.46	13.71
video 3	5.70	0.94	14.63
mean	4.82 +/- 0.473	1.15 +/- 0.157	14.10 +/-0.273

The 60% sucrose solution was also tested in hypergravity. Figure 24 shows the viscosity of the solution for a time lag from 1 to 33 (which is about 1s) for 1 video per g levels. It appears that the viscosity decreases with gravity level. We expect this outcome to be caused by increasing temperatures in the samples over time as the sample at 10g has been illuminated for 1.5 hours compared to the sample at 1g. The temperature increase is expected to be more than the temperature rise (from 20.7°C to 22.0 °C) by the incubator. The measured particle size for the recordings with 60% sucrose solution in hypergravity is shown in Figure 25. The measured particle size seems to increase with gravity level which could

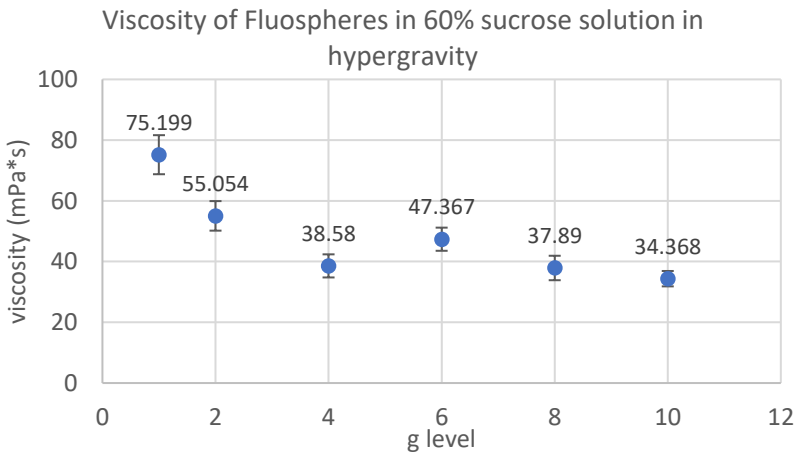

Figure 24. *Viscosity of 60% sucrose solution with Fluospheres® at different gravity levels. For each gravity level the first 33 frames for 1 video are analysed. The temperature gradually increases from 20.7°C to 22.0 °C.*

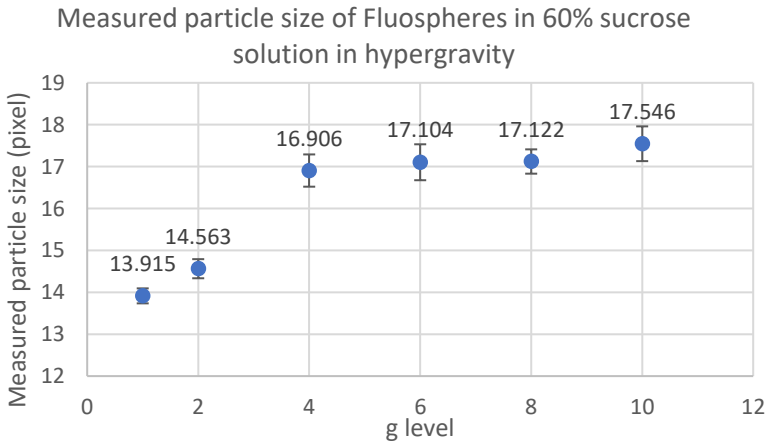

Figure 25. *Calculated particle size of 60% sucrose solution with Fluospheres® at different gravity levels. For each gravity level the first 33 frames for 1 video are analysed. The temperature gradually increases from 20.7°C to 22.0 °C.*

be caused by the increasing difficulty to track the particle as the LDC start to shake more vigorously with increasing g level.

Hela cells in hypergravity

Three consecutive gravity sequences from 1 to 12g have been executed with for each sequence a selected Hela cell. The three different sequences are referred to as S1, S2 and S3. All MSDs for each cell and gravity level can be found in the Supplemental Information. The viscosity of each Hela cell in different gravity levels along with the image of the selected cell area is provided in Figure 26a for S1, Figure26b for S2, and Figure26c for S3. Analysing the three viscosity plots there seems to be a trend for which the viscosity increases up till 4g after which it decreases. The viscosity measurements at 1g before and after the hypergravity treatment appear to vary between the three Hela cells. S1 and S2 start at similar viscosities at 1g but while the viscosity of S1 after the experiment seems to have dropped, the viscosity of S2 post-hypergravity treatment appears strongly increased. Furthermore, the viscosity of S3 start at a relatively high value compared to S1 and S2. S3 still seems to show a drop at 6g, after which it appears to rise again, and the post experiment value at 1g seems to be almost the same as the starting viscosity. While it was originally planned to incorporate 14g in the gravity sequence as well, videos were too blurry to perform any analysis.

The logarithmic exponent α in different gravity levels for each cell is provided in Figure 27a for S1, Figure27b for S2, and Figure27c for S3. It appears that α decreases up to about 4g after which it appears to fluctuate. For both S2 and S3 the post hypergravity logarithmic exponent seems to be decreased, while for S1 it appears to have increased to 1.

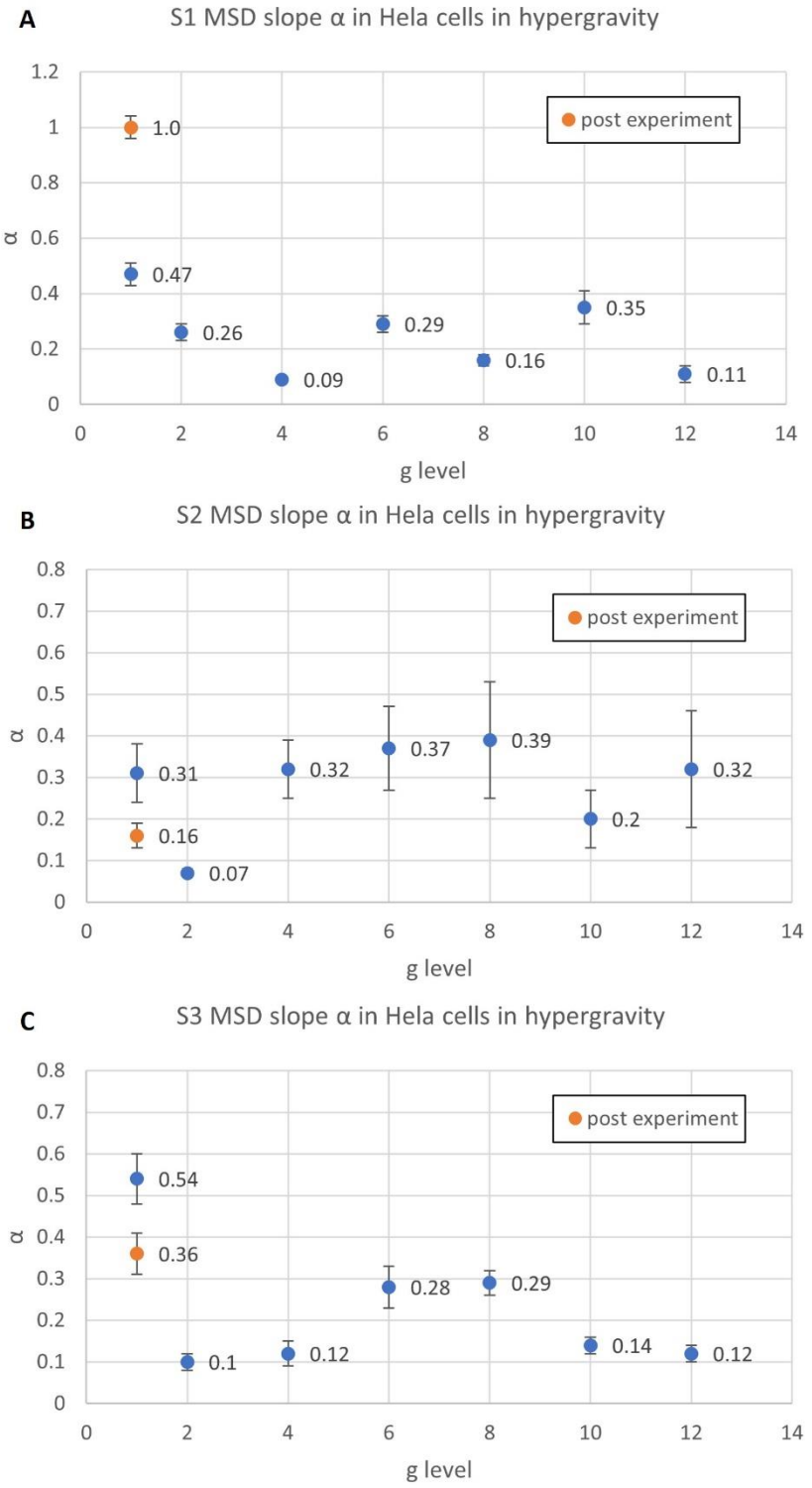

Figure 27. *The logarithmic exponent α for the MSD plots of Hela cells in different gravity levels at 60x zoom with background = 35, threshold =50, and Gaussian width = 5.0. The orange dots are the measurements taken at 1 g after completing the hypergravity sequences. (A) Sequence 1 (S1) Hela cells analysed in hypergravity at 24.8°C for which at least 28 particles were tracked, and the mean particle size is 13.7 +/- 0.16 pixels. (B) Sequence 2 (S2) Hela cells analysed in hypergravity at 25.2°C for which at least 7 particles were tracked, and the mean particle size is 14.6 +/- 0.31 pixels. (C) Sequence 3 (S3) Hela cells analysed in hypergravity at 24.3°C for which at least 13 particles were tracked, and the mean particle size is 12.7 +/- 0.37 pixels.*

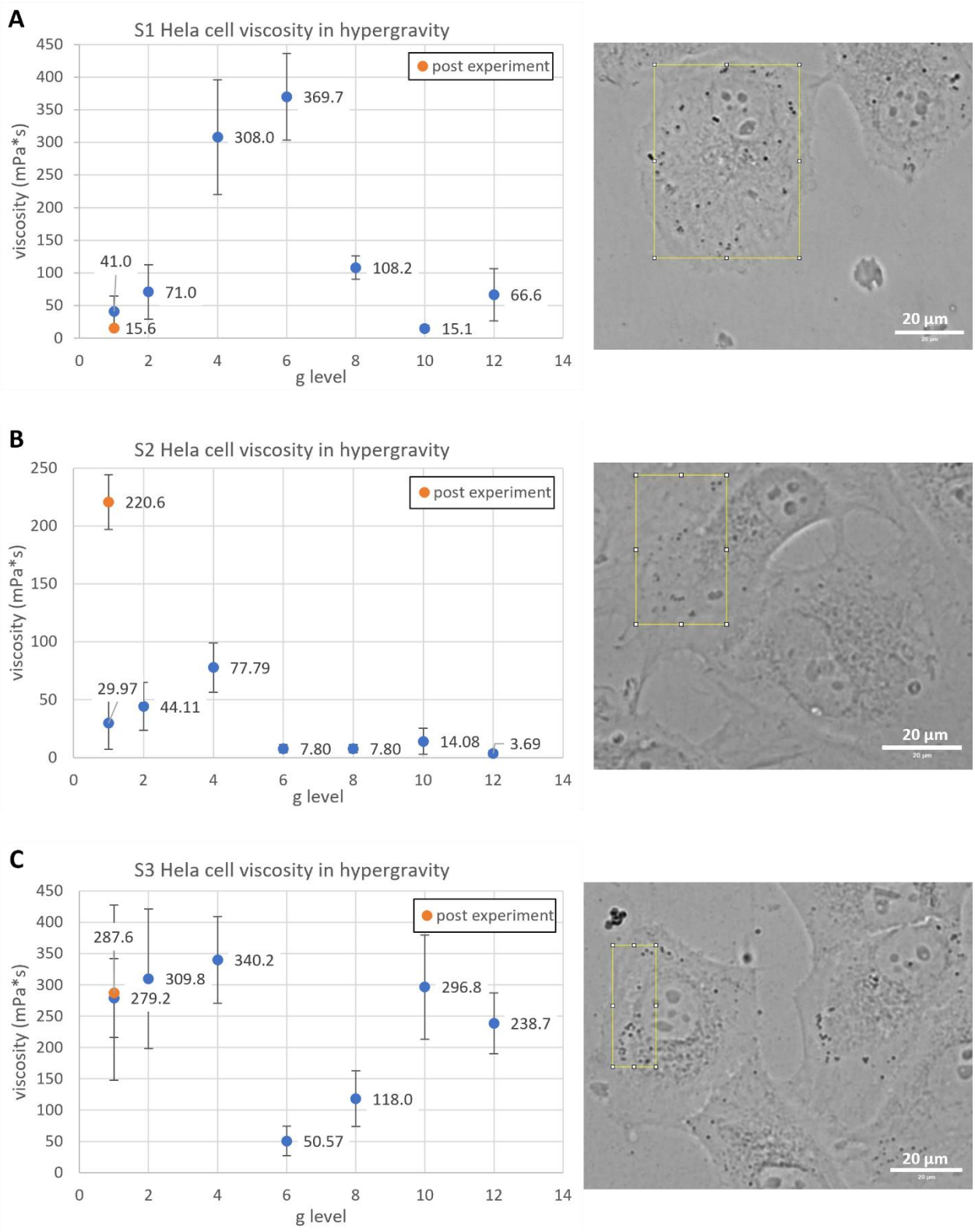

Figure 26. *Viscosity of Hela cells in different gravity levels at 60x zoom with background = 35, threshold =50, and Gaussian width = 5.0. The orange dots are the measurements taken at 1 g after completing the hypergravity sequences. Next to the plots an image of the cell of that specific sequence is displayed and in yellow the analysed area with unidentified particles. (A) Sequence 1 (S1) Hela cells analysed in hypergravity at 24.8°C for which at least 28 particles were tracked, and the mean particle size is 13.7 +/- 0.16 pixels. (B) Sequence 2 (S2) Hela cells analysed in hypergravity at 25.2°C for which at least 7 particles were tracked, and the mean particle size is 14.6 +/- 0.31 pixels. (C) Sequence 3 (S3) Hela cells analysed in hypergravity at 24.3°C for which at least 13 particles were tracked, and the mean particle size is 12.7 +/- 0.37 pixels.*

Although it was impossible to make recordings for the samples in Figure 26 above 12g, an earlier pilot experiment I conducted early in the thesis project in 15g was successful. For this experiment Hela cells were kept at 15g and a video of a cell in the sample was made at 1g, at 15 g after 10 minutes, after 42 minutes, and after 100 minutes. The results are plotted in Figure 28. The viscosity seems to decrease after which it appears recovered to some extent to its original viscosity after 100 min. However, the error bars are rather large, which is at least partly caused by looking at different cells for each time point.

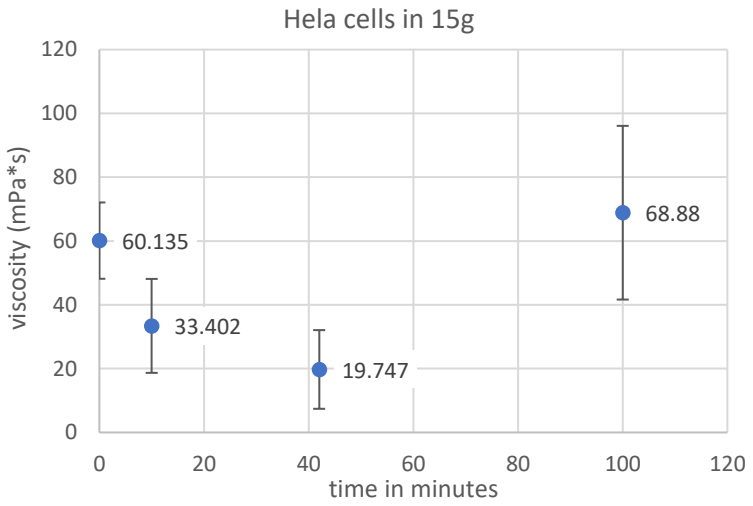

Figure 28. *Viscosity of the various Hela cells in 1g (time=0) and at 15g for different periods spent in hypergravity at room temperature for which at least 13 particles were tracked, and the mean particle size is 14.4 +/- 1.88 pixels. The background = 35, threshold =50, and Gaussian width = 5.0.*

4 Discussion

To test if the viscosity of cells alters in hypergravity and if it can be measured by Single Particle Tracking, the SPT program was adjusted, validated with Fluospheres® in sucrose after which it was applied to Hela cells experiencing gravity levels from 1 to 15g.

Validation test

Validation of the SPT program

The adjusted SPT program was able to detect the Fluospheres® and estimated a realistic viscosity and particle size. For the 60% sucrose solution the mean viscosity of three videos was 53.11 +/- 4.0 mPa*s which closely agrees with what is found in literature[36 37]. The apparent viscosity of the 30% sucrose solution was higher than the expected viscosity[36] of 2.997 mPa*s. For the preparation of the 60% sucrose a large batch was prepared in a 50 ml Erlenmeyer flask, while the mixture of the 30% sucrose was performed with 0.5 ml of the 60% sucrose solution and 0.5 ml of milli-Q. It is suspected that the large batch allowed for a more accurate sucrose concentration, while the small quantities for the 30% solution induced more inaccuracy resulting in a slightly higher concentration of sucrose for which only a 6% sucrose increment is sufficient to obtain the viscosity[36] of 4.82 +/- 0.473 mPa*s.

Temperature variations

The mean particle width for both solutions seems to be slightly higher than the expected 13.75 pixel which is the actual size of the Fluospheres®. Interestingly, the first videos from either the 60% solution or the 30% solution appear to better estimate the particle size than the following recordings. Upon further inspection of the videos, it seems that more drift is present in later videos and that some particles tend to get out of focus during the recording. After performing temperature measurements on the EVOS microscope it appears that the microscope can elevate the temperature with the GFP filter between 0.5 and 1.4 °C for the 60x and 40x zoom respectively. Furthermore, the closed system slowly increased in temperature during the experiment and the incubator does not

indicate the actual temperature. It is expected that the heat of the microscope induces local currents which become more severe in time and result in an accelerated drift leading to blurry images and evidently a larger mean particle size.
The drift does not interfere with the calculation for Brownian diffusion as the selected MSD equation for the validation test includes a velocity term which captures most of the motion resulting in the majority of the logarithmic exponent α to remain near 1.

Fluospheres® in hypergravity
The validation test was also performed in hypergravity to check if the drift correction interferes with the MSD. A drift correction was required to filter out vibrations which tend to aggravate with increasing g-level. The source of these vibrations is yet to be determined but we speculate that they are introduced by the LDC. The drift correction is able to filter out the majority of these vibrations without compromising the MSD as the viscosity of the probes in sucrose seem to decrease with gravity level rather than to increase. If the drift correction would adjust the MSD a more constricted motion is expected resulting in a higher viscosity. It is assumed that the viscosity of sucrose in hypergravity remains moderately consistent aside from a small, but neglectable, elevation created by increased friction from the probes moving through the sucrose.
The decrease in viscosity in hypergravity is suspected to be caused by a rising temperature. The entire microscope setup is placed in the gondola forming a closed system which slowly heats up. It was shown that without illumination, just turning on the microscope, the temperature in the gondola can easily reach 25 °C. Additional heat by illumination introduced over the course of the experiment could readily increase the temperature to about 30 °C for the final videos taken at 10g. At 30 °C the viscosity[37] of the 60% sucrose solution is expected to be 35.2 mPa*s. This number is close to the value of 34.368 mPa*s found in our results for 10g.
The mean particle size seems to increase as well in hypergravity. It is suspected that the combination of increasing drift due to the temperature rise and the aggravated shaking with gravity level, causes the particle to be more out of focus with increasing gravity level.

Hela cells

Hela cell viscosity in hypergravity
All three viscosity graphs for the three Hela cells appear to have a trend for which the viscosity seems to increase up to 4g after which it decreases again. Simultaneously, the logarithmic exponent α appears to decrease to about 4g after which it increases. A lower α indicates more confined diffusion.
The increase in viscosity and the decrease of the logarithmic exponent alpha could be a result of hypergravity amongst other things which will be discussed later.
Although little research on cell viscosity is performed in hypergravity, as to the best of my knowledge, Woodcock et al. [10] observed increased membrane viscosity in hypergravity. On the other side of the gravity spectrum, the viscosity and stiffness of endothelial cells seem to decrease in simulated microgravity[12]. Studies indicate cell stiffening in response to force application due to actin recruitment[38]. Cell stiffening due to cytoskeleton alterations is also observed for skeletal muscles fibres in 2g, while cell stiffness decreases in cardiomyocytes[18].
Another consideration regarding the potential increased cell viscosity is cell flattening. Gravity levels ranging between 2 to 3g can already reduce the cell height with 30 to 50%[39]. If the cell area does not adjust accordingly, higher molecular crowding can result in an increase in cytoplasmic viscosity and stiffness due to a rise in solid volume fraction[40].

Hela cell viscosity pre- and post hypergravity treatment

Comparing the pre- and post hypergravity measurements for the Hela cells, cell S1 and cell S2 have similar pre-hypergravity treatment viscosities, while S3 starts off with an almost tenfold greater viscosity. Aside from other suggestions of variations in the viscosity mentioned in the next paragraph, I suggest that recovery time of the cell might be critical in this case. While there was an interval of an hour between S1 and S2, there was none between S2 and S3. Hence, the cells might require a certain recovery time to return to their pre-hypergravity viscosity. Myoblastic cells seem to stiffen in response to force application in about 600s but ranging from 90s to 2000s, so a delay can be expected as well during cell softening[38]. In fact, to ensure full cellular relaxation after hypergravity treatment Woodcock et al.[10] waited at least 3 hours as an elevated membrane viscosity was still present after 45 minutes in 1g.

The high starting viscosity of S3 could also be a result in the relatively small difference between pre- and post-hypergravity measurements as the cell was already adjusted to higher g levels. In fact, the post-hypergravity viscosity of S2 is in the same range as the starting viscosity of S3. In S2 the viscosity is much higher after the hypergravity treatment, while for S1 the viscosity seemed to be decreased after the hypergravity treatment. Consulting the logarithmic α plots, it can be observed that the post-experiment α is 1.0, which is rather high compared to the other values in the plot of S1 and the α plots of the other cells. A logarithmic exponent of 1 indicates perfect Brownian motion. More cells need to be investigated to confirm that this is an outlier.

Viscosity measurements interpretation

We are cautious about our statements as only three Hela cells have been analysed in hypergravity.

The outcome of the experiment could also have been influenced by the suboptimal temperature and CO_2. Due to limited control in temperature variations as mentioned earlier, we opted for an approach in which the LDC and the EVOS microscope run for several hours to achieve a rather constant temperature of about 25°C. If the incubator was set on 37°C instead, temperatures can easily rise above 40°C, resulting in Hela cell apoptosis[41]. CO_2 should have been controlled as well, however, due to complications with the calibration of the EVOS microscope a higher resolution was achieved without the lid of the EVOS incubator. Without a lid it is not possible to control the CO_2 of the cells.

Additionally, the three cells, aside from displaying a similar trend, all showed unique behaviour. The Hela cells were individually analysed in different g levels as cells are living, complex systems. In fact, even within the cell large variations of viscosity are found due to the heterogeneous nature of the cell[24]. For example, in mouse macrophages the viscosity ranges between 1.0 and 2.21 mPa*s in a single cell[42]. However, it is argued by some that the differences within the cell are as large as the changes between the cells as the intracellular standard deviation of viscosity within one Hela cell was found to be 12.6% and the standard deviation between Hela cells 12.7%[43]. Furthermore, it is debated wheter the cell cycle also affects the viscosity. While some suggest increased viscoelastic fluidity during division[44], others do not observe a change between different stages of the cell cycle in Hela cells[45]. Moreover, as the tracking particles have not been identified, it might also be the case that different types of particles are tracked between cells and within the cell itself, causing large variations in viscosity. In fact, it appears that the measured viscosity depends on the size of the tracking particle[43].

LDC vibrations

Analysing the single cell plots, an increase to about 4g was observed after which viscosity seems to diminish. The opposite seems to occur for the logarithmic exponent α that decreases up to 4g after which it increases again.
I speculate that the reduction in viscosity and the increase of α is an artefact as the recordings from 6g onwards show severe shaking within the image. The drift correction can adjust for oscillation as shown in the validation test, but the when the displacement is faster than the exposure time a dot appears in the image as a stripe and the drift correction fails to adjust for this. The recordings with the Fluospheres® in 60% sucrose appear to be less prone to this phenomenon compared to the videos with cells and the 30% sucrose solution. I speculate that the high viscosity of the sucrose solution aids to suppress the oscillations, while the more fluid solution and the cells attached to the slide are more susceptible to the vibrations. Furthermore, the sucrose solution has more datapoints as per field of view about 150 particles are tracked, whereas for the cells only a small portion of the video (the part with the endogenous particles) is examined which tracks at most 50 particles. The number of tracked particles reduces for all recordings with increasing hypergravity as it becomes more difficult to track the particle, thereby also decreasing the reliability.

Pilot experiment
Although recordings above 12g were not feasible due to excessive vibrations, a previous pilot experiment, I performed early in the thesis project, still allowed to take recordings of Hela cells at 15g. It appears that between the 15g experiment and the following experiments some elements changed which resulted in more vigorous shaking in the recordings. It is unclear whether this additional disturbance is caused by a mechanical error in de LDC or in the EVOS microscope. While there appears to be a decrease in viscosity over time, the error bars are too large to make any suggestions. For this experiment various Hela cells were used for different time stamps, and the temperature and CO_2 were not controlled which together result in large errors.

Outlook
In this section recommendations are given to improve the future research on this project.

Cell recommendations
Foremost, a higher population of cells needs to be investigated to improve statistics and to be able to make profound claims of the effect of hypergravity on cell viscosity. Furthermore, the type of cell needs to be revised or more cell types need to be studied as cancer cells behave differently in topics such as stiffness compared to healthy cells[46]. In addition, other tracking particles in the cell for which the identity is known are preferred to secure Stokes' law assumptions of a rigid and spherical particle and to improve the viscosity calculations.

Viscosity calculations improvement
Obtained viscosity values depend heavily on applied method[21], cell type[22], external stimuli and even location in the cell[23]. The viscosity values found for this project are, in addition to the above, also subjected to large assumptions that oversimplify the complex, heterogenous, crowded, and viscoelastic nature of cells. Although this simple model suffices for the objective of this study which is to determine any change, to improve the data the complex shear modulus and creep compliance should be used to capture the viscoelastic behaviour of the cell.
The tracking particles will not move freely though the cytoplasm. Instead, due to their size ranging from 1.01 to 1.17 µm which is larger than the average pore size of the cytoskeleton meshwork (20-40 nm)[34], they will encounter resistance from the filamentous meshwork, resulting in a perceived viscosity that reflect the viscoelasticity of the cytoskeleton network[27]. This represents a non-Newtonian environment in which the viscosity is time-dependent resulting in an anomalous sub-

diffusion rather than normal diffusion[19]. Therefore, it is recommended to incorporate the deformability of the cytoskeleton by calculating the creep compliance from the MSD of the tracking particles[47]. The creep compliance is often considered sufficient as most mechanical information is provided in the amplitude and the time-scale dependence of the compliance[33]. In addition, the frequency-dependent complex shear modulus can be calculated by projecting the MSD to the frequency-dependent Fourier domain after which the generalized, frequency-dependent Stokes-Einstein relationship is applied[19,47]. The real part of the complex shear modulus is the elastic behaviour (storage modulus), and the imaginary part is the viscous behaviour (loss modulus). Hence, I also recommended to calculate the frequency-dependent complex shear modulus.

Experiment setup adjustment

Future experiments would benefit from identifying the source of the complication that induces the additional oscillations in the LDC. Not only will this improve the accuracy of the trajectories of the particles, but it would also allow to investigate higher g levels. Furthermore, we advise to ensure a constant temperature in the gondola by removing heat sources or adding active cooling systems. The inaccuracy of the temperature indication by the EVOS incubator also needs to be resolved. The validation test was performed with fluorescent particles, but the GFP filter of the microscope seemed to induce local heat currents. Therefore, it is recommended to perform the validation test with white light while accurately monitoring the temperature. The calibration issue of the EVOS microscope was for the majority resolved but needs to improve such that the lid of the incubator does not pose a problem for the resolution. This would allow to actively control and optimize the CO_2 values for Hela cells.

We advise to investigate if the cells have a certain recovery time by taking several measurements post hypergravity. If they indeed require time to recover it should be accounted for in the test setup. Samples can then either be used once or a waiting time between tests need to be incorporated. The latter allows for a sample to be reused in multiple hypergravity sequences as there seem to be no permanent changes in the cell which endured hypergravity treatment[10].

Finally, for future experiments it would be interesting to incorporate drugs like Jasplakinolide and Latrunculin-B that alter the cytoskeleton as some studies related elevated rigidity to increased actin recruitment[38].

5 CONCLUSION

Deducting the change in viscosity in hypergravity with Single Particle Tracking is possible, yet still requires significant improvement. The viscosity of cells seems to change during the hypergravity experiments, but it is to be determined whether this is an effect of hypergravity or due to other factors. It is recommended to investigate more cells (types), improve the viscosity calculations by incorporating creep compliance and the complex shear modulus, determine the cell's recovery time after hypergravity by measuring several hours post experiment, minimize temperature variations by incorporating active cooling systems, adjust the cell's environment to the physiological condition temperature and CO_2 concentration, solve or mitigate the LDC vibrations, and incorporate cytoskeletal drugs like Jasplakinolide and Latrunculin-B to investigate the contribution of the cytoskeleton in the viscosity.

6 ACKNOWLEDGEMENTS

I am incredibly grateful for doing this exciting project and the immense support I received from everyone involved. All showed huge enthusiasm and had a flexible attitude which was definitely welcome in a project involving many parties. I would like to express my deepest gratitude to Dr. ing. Jack J.W.A. van Loon for arranging this out-of-this-world thesis project opportunity for me. His daily support, guidance and knowledge throughout the project was very appreciated and inspires me to continue my career as a scientific researcher. I am also very grateful for the help of Prof. dr. Thomas Schmidt who guided and taught me to work with the SPT software and for his impeccable patience to improve my knowledge in statistics. This amazing opportunity would not have been possible without the support of Prof. dr. Gijsje Koenderink who supervised the project and gave excellent critical feedback. Special thanks to Robert Lindner and the technical assistance of Alan Dowson from the ESA TEC-MMG Life Support and Physical Sciences Laboratory for providing all the necessary equipment, space, and chemicals to perform this thesis. I would like to extend my sincere thanks to faculty of Dentistry (ACTA) at the VU University Amsterdam for hosting me and Jin Jianfeng from the Department of Oral Cell Biology for providing the MC-3T3 cells. Many thanks also go to Rick Rodrigues de Mercado who helped me solve many tedious MATLAB programming issues and provided the Hela cells. Lastly, I did like to thank James Conboy for providing the Fluospheres® and for the discussion on the logarithmic MSD plots.

7 REFERENCES

1. Ruthardt N, Lamb DC, Brauchle C. Single-particle tracking as a quantitative microscopy-based approach to unravel cell entry mechanisms of viruses and pharmaceutical nanoparticles. *Molecular therapy : the journal of the American Society of Gene Therapy.* 2011;19(7):1199-1211.
2. Moeendarbary E, Harris AR. Cell mechanics: principles, practices, and prospects. *Wiley Interdiscip Rev Syst Biol Med.* 2014;6(5):371-388.
3. Lisitsa AE, Sukovatyi LA, Bartsev SI, Deeva AA, Kratasyuk VA, Nemtseva EV. Mechanisms of Viscous Media Effects on Elementary Steps of Bacterial Bioluminescent Reaction. *Int J Mol Sci.* 2021;22(16).
4. Zheng K, Jensen TP, Savtchenko LP, Levitt JA, Suhling K, Rusakov DA. Nanoscale diffusion in the synaptic cleft and beyond measured with time-resolved fluorescence anisotropy imaging. *Sci Rep.* 2017;7:42022.
5. Nadiv O, Shinitzky M, Manu H, et al. Elevated protein tyrosine phosphatase activity and increased membrane viscosity are associated with impaired activation of the insulin receptor kinase in old rats. *Biochem J.* 1994;298 (Pt 2)(Pt 2):443-450.
6. Shen W, Wang P, Xie Z, et al. A bifunctional probe reveals increased viscosity and hydrogen sulfide in zebra fish model of Parkinson's disease. *Talanta.* 2021;234:122621.
7. Pan X, Wang C, Zhao C, et al. Assessment of cancer cell migration using a viscosity-sensitive fluorescent probe. *Chemical Communications.* 2022;58(29):4663-4666.
8. Persson LB, Ambati VS, Brandman O. Cellular Control of Viscosity Counters Changes in Temperature and Energy Availability. *Cell.* 2020;183(6):1572-1585.e1516.
9. Hughes-Fulford M. Altered cell function in microgravity. *Experimental Gerontology.* 1991;26(2-3):247-256.
10. Woodcock EM, Girvan P, Eckert J, et al. Measuring Intracellular Viscosity in Conditions of Hypergravity. *Biophysical Journal.* 2019;116(10):1984-1993.
11. Sieber M, Hanke W, Kohn FPM. Modification of Membrane Fluidity by Gravity. *Open Journal of Biophysics.* 2014;04(04):105-111.

12. Janmaleki M, Pachenari M, Seyedpour SM, Shahghadami R, Sanati-Nezhad A. Impact of Simulated Microgravity on Cytoskeleton and Viscoelastic Properties of Endothelial Cell. *Scientific Reports.* 2016;6(1):32418.
13. Callister WD, Rethwisch DG. *Materials Science and Engineering.* 9 ed: Wiley; 2014.
14. Wubshet NH, Arreguin-Martinez E, Nail M, et al. Simulating microgravity using a random positioning machine for inducing cellular responses to mechanotransduction in human osteoblasts. *Review of Scientific Instruments.* 2021;92(11).
15. Ogneva IV. Transversal stiffness of fibers and desmin content in leg muscles of rats under gravitational unloading of various durations. *J Appl Physiol (1985).* 2010;109(6):1702-1709.
16. Ogneva IV. Transversal Stiffness and Beta-Actin and Alpha-Actinin-4 Content of the M. Soleus Fibers in the Conditions of a 3-Day Reloading after 14-Day Gravitational Unloading. *Journal of Biomedicine and Biotechnology.* 2011;2011:393405.
17. Mao X, Chen Z, Luo Q, Zhang B, Song G. Simulated microgravity inhibits the migration of mesenchymal stem cells by remodeling actin cytoskeleton and increasing cell stiffness. *Cytotechnology.* 2016;68(6):2235-2243.
18. Ogneva IV, Gnyubkin V, Laroche N, Maximova MV, Larina IM, Vico L. Structure of the cortical cytoskeleton in fibers of postural muscles and cardiomyocytes of mice after 30-day 2-g centrifugation. *J Appl Physiol (1985).* 2015;118(5):613-623.
19. Selvaggi L, Salemme M, Vaccaro C, et al. Multiple-Particle-Tracking to investigate viscoelastic properties in living cells. *Methods.* 2010;51(1):20-26.
20. Schmidt T, Schutz GJ, Baumgartner W, Gruber HJ, Schindler H. Imaging of single molecule diffusion. *Proc Natl Acad Sci U S A.* 1996;93(7):2926-2929.
21. Hoffman BD, Massiera G, Van Citters KM, Crocker JC. The consensus mechanics of cultured mammalian cells. *Proc Natl Acad Sci U S A.* 2006;103(27):10259-10264.
22. Wirtz D. Particle-tracking microrheology of living cells: principles and applications. *Annu Rev Biophys.* 2009;38:301-326.
23. Yamada S, Wirtz D, Kuo SC. Mechanics of living cells measured by laser tracking microrheology. *Biophys J.* 2000;78(4):1736-1747.
24. Heidemann SR, Wirtz D. Towards a regional approach to cell mechanics. *Trends Cell Biol.* 2004;14(4):160-166.
25. Bobroff N. Position measurement with a resolution and noise-limited instrument. *Review of Scientific Instruments.* 1986;57(6):1152-1157.
26. Kusumi A, Sako Y, Yamamoto M. Confined Lateral Diffusion of Membrane-Receptors as Studied by Single-Particle Tracking (Nanovid Microscopy) - Effects of Calcium-Induced Differentiation in Cultured Epithelial-Cells. *Biophysical Journal.* 1993;65(5):2021-2040.
27. Chen YQ, Kuo CY, Wei MT, et al. Intracellular viscoelasticity of HeLa cells during cell division studied by video particle-tracking microrheology. *J Biomed Opt.* 2014;19(1):011008.
28. Hofling F, Franosch T. Anomalous transport in the crowded world of biological cells. *Rep Prog Phys.* 2013;76(4):046602.
29. Gal N, Lechtman-Goldstein D, Weihs D. Particle tracking in living cells: a review of the mean square displacement method and beyond. *Rheologica Acta.* 2013;52(5):425-443.
30. Vanapalli SA, Li Y, Mugele F, Duits MH. On the origins of the universal dynamics of endogenous granules in mammalian cells. *Mol Cell Biomech.* 2009;6(4):191-201.
31. Lommerse PHM, Snaar-Jagalska BE, Spaink HP, Schmidt T. Single-molecule diffusion measurements of H-Ras at the plasma membrane of live cells reveal microdomain localization upon activation. *Journal of Cell Science.* 2005;118(9):1799-1809.
32. Einstein A. Zur Theorie der Brownschen Bewegung. *Annalen der Physik.* 1906;324(2):371-381.
33. Tseng Y, Kole TP, Wirtz D. Micromechanical mapping of live cells by multiple-particle-tracking microrheology. *Biophys J.* 2002;83(6):3162-3176.
34. Luby-Phelps K, Taylor DL, Lanni F. Probing the structure of cytoplasm. *J Cell Biol.* 1986;102(6):2015-2022.

35. Presley AD, Fuller KM, Arriaga EA. MitoTracker Green labeling of mitochondrial proteins and their subsequent analysis by capillary electrophoresis with laser-induced fluorescence detection. *J Chromatogr B Analyt Technol Biomed Life Sci.* 2003;793(1):141-150.
36. Swindells JF, Snyder CF, Hardy RC, Golden PE. *Supplement to National Bureau of Standards Circular No. 440: Viscosities of Sucrose Solutions at Various Temperatures : Tables of Recalculated Values.* Washington D.C: U.S. Department of Commerce, National Bureau of Standards; 1958.
37. Telis VRN, Telis-Romero J, Mazzotti HB, Gabas AL. Viscosity of Aqueous Carbohydrate Solutions at Different Temperatures and Concentrations. *International Journal of Food Properties.* 2007;10(1):185-195.
38. Icard-Arcizet D, Cardoso O, Richert A, Hénon S. Cell stiffening in response to external stress is correlated to actin recruitment. *Biophys J.* 2008;94(7):2906-2913.
39. van Loon JJ, van Laar MC, Korterik JP, et al. An atomic force microscope operating at hypergravity for in situ measurement of cellular mechano-response. *J Microsc.* 2009;233(2):234-243.
40. Efremov YM, Grebenik EA, Sharipov RR, et al. Viscoelasticity and Volume of Cortical Neurons under Glutamate Excitotoxicity and Osmotic Challenges. *Biophys J.* 2020;119(9):1712-1723.
41. Bettaieb A, Averill-Bates DA. Thermotolerance induced at a mild temperature of 40°C alleviates heat shock-induced ER stress and apoptosis in HeLa cells. *Biochimica et Biophysica Acta (BBA) - Molecular Cell Research.* 2015;1853(1):52-62.
42. Parker WC, Chakraborty N, Vrikkis R, Elliott G, Smith S, Moyer PJ. High-resolution intracellular viscosity measurement using time-dependent fluorescence anisotropy. *Opt Express.* 2010;18(16):16607-16617.
43. Kwapiszewska K, Szczepański K, Kalwarczyk T, et al. Nanoscale Viscosity of Cytoplasm Is Conserved in Human Cell Lines. *The Journal of Physical Chemistry Letters.* 2020;11(16):6914-6920.
44. Hurst S, Vos BE, Brandt M, Betz T. Intracellular softening and increased viscoelastic fluidity during division. *Nature Physics.* 2021;17(11):1270-1276.
45. Szczepański K, Kwapiszewska K, Hołyst R. Stability of cytoplasmic nanoviscosity during cell cycle of HeLa cells synchronized with Aphidicolin. *Scientific Reports.* 2019;9(1):16486.
46. Grady ME, Composto RJ, Eckmann DM. Cell elasticity with altered cytoskeletal architectures across multiple cell types. *J Mech Behav Biomed Mater.* 2016;61:197-207.
47. Dong C, Zahir N, Konstantopoulos K. *Biomechanics in Oncology.* Vol 1092: Springer International Publishing; 2018.